Jingxian Yu, John R. Horsley, Andrew D. Abell
Turning electron transfer 'on-off' in peptides through side-bridge gating
Electrochimica Acta, 2016; 209:65-74

Final publication at http://dx.doi.org/10.1016/j.electacta.2016.05.067

Turning electron transfer 'on-off' in peptides through side-bridge gating

Jingxian Yu*, John R. Horsley, Andrew D. Abell*

ARC Centre of Excellence for Nanoscale BioPhotonics (CNBP), School of Physical Sciences, The University of Adelaide, SA 5005, Australia

*Corresponding author e-mail address: jingxian.yu@adelaide.edu.au and andrew.abell@adelaide.edu.au.

ABSTRACT

Electrochemical studies are reported on a series of peptides to determine the influence of different side-chains and backbone rigidity on electron transfer, to progress the field of molecular electronics. Specifically, these peptides share either a common helical or β-strand conformation to cover a range of secondary structures, to fully investigate the influence of backbone rigidity. Two types of side-chain tethers, either triazole-containing or alkene-containing, are also compared to investigate these effects on electron transfer. Our results showed that the observed formal potentials (E_o) and apparent electron transfer rate constants (k_{et}) fall into two distinct groups. The peptides constrained via a side-chain tether exhibited high formal potentials and low electron transfer rate constants, whereas the linear peptides displayed low formal potentials and high electron transfer rate constants. This was found to occur irrespective of the backbone conformation, or the nature of the side-chain constraint. The vast formal potential shifts (as much as 482 mV) and the large disparity in the electron transfer rate constants (as much as 97%) between the constrained and linear peptides, provides two distinct states (i.e. on/off) with a sizeable differential, which is ideal for the design of molecular switches.

Keywords: Electron transfer in peptides, side-bridge, 3_{10}-helical, β-strand, click chemistry, ring-closing metathesis.

1. Introduction

Since individual molecules were proposed as active electronic components by Aviram and Ratner in the early 1970s [1], molecular electronics has been considered as a possible revolutionary successor to conventional semiconducting electronics [2]. Tremendous research efforts have been made to explore the properties and device opportunities of single molecules [3]. To date, molecular components such as switches, diodes and transistors have been demonstrated using functionalized conjugated molecules [4-6]. However, going beyond simple molecular systems to more complicated ones exhibiting multiple functionalities, such as those with molecular selectivity and long-term stability, necessitates overcoming formidable obstacles [7]. Electron transfer in proteins has played a crucial role in energy conversion and storage in all living organisms for almost two billion years [8], thus providing an opportunity for one to mimic nature for applications such as molecular electronics. Synthetic peptides present as ideal candidates for such a purpose [9, 10], due to the complex nature of even the simplest protein. Peptides are particularly useful for studying charge transfer mechanisms and function as they can be explicitly designed to conform to well-defined secondary structures such as β-strands and helices, where this is known to influence the efficiency of electron transfer [11-14]. They can self assemble on a conducting surface such as gold or silicon [15, 16], while also having an ability to be specifically functionalized along their backbone to enable precision-branching. This then promotes the development of stable and well-defined three-dimensional molecular circuitry [17, 18]. Peptides can also be derivatized with ‘smart’ groups such as photo-or electro-active components [19, 20], affording the peptide scaffold with specific functionalities for discrete applications in molecular electronics [21, 22]. However, a more detailed understanding on

exactly what controls the mechanisms and efficiency of electron transfer in peptides is required before this promise can be fully realized.

The introduction of a macrocyclic constraint has been shown to increase backbone rigidity [23, 24], which restricts the necessary torsional motion required for facile electron transfer through the peptide [25, 26]. This then provides a level of control over electron transfer in peptides. Moreover, manipulation of the chemical composition of the side-bridge may provide additional control over the electronic properties of the peptide [26]. Hence, studies are needed to further investigate these effects by comparing peptides with alternative side-bridge constraints, which afford varying ring sizes and chemical compositions. Here we present electrochemical studies on a series of synthetic peptides **1**-**8** to determine the influence of these effects on electron transfer, in isolation from other factors, such as chain length [27-29], dipole orientation [30, 31] and the associated hydrogen bonding [32, 33] that are known to influence electron transfer. Peptides **1**-**4**, as shown in Fig. 1 contain the geminally disubstituted residue, α-aminoisobutyric acids (Aib). They were used in the study since relatively short oligomers of Aib (3 or more units) are known to form predictable and particularly stable 3_{10}-helical structures [28, 31, 34, 35]. Thus, Aib-rich peptides made ideal model systems for investigating electrochemical mechanisms and kinetics in solution phase, demonstrated by previous pioneering work in this area [28, 29]. Peptide **2** comprises a triazole-containing side-chain, while an alkene-containing side-chain is located at the same position in peptide **4**. The backbones of peptides **1** and **3** were further constrained into a 3_{10}-helix with a side-chain linking the *i* and *i*+3 residues, introduced by Huisgen cycloaddition [23] and ring-closing metathesis [36] respectively. This results in additional conformational rigidity of their backbones. Peptides **5**-**8**, as shown in Fig. 2, share a common β-strand

conformation. Peptide **6** comprises a triazole-containing side-chain, while an alkene-containing side-chain is situated in the same location for peptide **8**. The backbones of peptides **5** and **7** were further constrained into a β-strand conformation, linking the *i* to *i*+2 residues with a triazole-containing and an alkene-containing tether respectively. Specifically, peptides with either a β-strand or helical conformation are studied to cover a range of secondary structures, to fully investigate influences of backbone rigidity while two types of side-chain tethers, either triazole-containing or alkene-containing, are also compared to look into these effects on electron transfer.

[Figure 1]

[Figure 2]

2. Experimental

2.1. Chemicals and synthesis

All amino acids and coupling reagents for peptide synthesis were purchased from either GL Biochem (Shanghai) Ltd, China or Sigma-Aldrich, Australia. All solvents were purchased from Merck and Chem Supply, Australia. All reagents and solvents were used without purification unless noted. The synthesis of triazole-containing 3_{10}-helical (**1** and **2**) [25] and β-strand peptides (**5** and **6**) [37] have been reported in our earlier publications. Detailed information on synthesis of ring-closing metathesis (RCM) macrocyclized peptides (**3** and **7**) and their linear analogues (**4** and **8**) have been previously reported [26].

2.2. Spectroscopic characterisations

Two-dimensional NMR experiments utilizing COSY, ROESY, HSQC and HMBC were obtained on a Varian Inova 600 MHz spectrometer. High resolution mass spectral data were analyzed using an Agilent Technologies 6200 series TOF LC/MS 6500 with an Agilent Technologies 1260 Infinity LC system, with a flow rate of 0.5 mL/min. Infrared spectra were collected on a Perkin Elmer Spectrum 100 FT-IR spectrometer, with attenuated total reflectance (ATR) imaging capabilities, fitted with a ZnSe crystal, with an average reading taken from 4 scans at 4 cm^{-1} resolution. Circular dichroism (CD) spectra were acquired with a JASCO J-815 CD spectrometer (JASCO, UK) using an optical cell of 0.1 cm optical path length at the residue concentration of 2.7 mM in methanol at 22°C.

2.3. Computational methods

The lowest energy conformers for all of the *N*-Boc protected peptides were determined in Gaussian 09, with tight convergence criteria using a hybrid B3LYP method with 6-31G** basis set for all C, H, N, O atoms, and Lanl2dz basis set for the Fe atom in order to define the backbone conformations of all constrained and unconstrained peptides. The *N*-protected peptides were used in these studies as free amines are known to give rise to unrealistic electrostatic interactions, resulting in unstable lowest energy conformers [38].

The geometry of each diabatic state was optimised using cDFT [39] as implemented in NWChem 6.1 [40]. Diabatic potential profiles were determined in acetonitrile solvent by assuming that during an electron transfer step the nuclear configuration changes smoothly between the optimised geometries of the diabatic states in which the excess electron is localised before and after electron transfer [25]. Thus, the energy of each of the two diabatic states along the electron transfer reaction coordinate was taken as the energy for geometries linearly interpolated between the optimised geometries of the two diabatic

states, with the excess electron localised to the part of the molecule corresponding to the diabatic state in question.

2.4. Preparation of ferrocene-derivatised peptide electrodes

P2-SWCNTs were functionalised using previously reported methods [41]. Shortened CNTs were then suspended in a solution of DMSO containing 0.2 mg mL^{-1} CNTs, 0.25 mg mL^{-1} DCC and 0.14 mg mL^{-1} DMAP. Polished flat gold disk electrodes were cleaned in 25 % v/v H_2O_2/ KOH (50 mM) for 20 min and then electrochemically cleaned by cycling between 0 and 1.5 V vs. Ag/AgCl in 50 mM KOH. This cleaning process yielded clean gold surfaces with peak separations of 59 mV in 1 mM $Ru(NH_3)_6^{+3/2}$ solution. The clean surfaces were then incubated in cysteamine for 24 h resulting in exposed amine groups. These substrates were then exposed to the functionalised SWCNTs/DMSO suspensions for 24 h, after which they were rinsed with propan-2-ol and dried under nitrogen flow. The surfaces were then exposed to 0.01 M ferrocene-derivatised peptide in DMF solution containing 0.5 M HATU and 0.5 M DIPEA for 48 h before being further rinsed and dried. A typical AFM image of vertically aligned single-walled carbon nanotube array/gold (SWCNTs/Au) electrode (50×50 μm^2) is shown in Fig. 3. The average height of single-walled nanotubes is 206.9 nm. SWCNTs/Au electrodes were used in this study to provide a high surface concentration of redox probes, with an associated significant increase in sensitivity and reproducibility of the electrochemical measurement over bare Au electrodes [41-43].

[Figure 3]

2.5. Electrochemical measurements

All electrochemical measurements were conducted on a CHI 650D Electrochemical Analyzer (CH Instruments Inc) with ohmic-drop correction at room temperature. When the conditions leading to large voltammogram distortions are unavoidable, the post measurement ohmic-drop corrections can be successfully applied through the electrochemical standard software programs to eliminate an error caused by the voltammograms distortion [44]. A peptide modified gold surface formed the working electrode, with a platinum mesh and Ag/AgCl wire used as the counter and reference electrodes, respectively. The Ag/AgCl reference electrode was calibrated after each experiment against the ferrocene / ferrocenium couple. Ferrocene-derivatized peptide electrodes were electrochemically characterized in 0.1 mol L^{-1} tetra-*n*-butylammoniumhexafluorophosphate ($TBAPF_6$) / CH_3CN solutions. The digitized and background-subtracted curves were analyzed using a Data Master 2003 program. Surface concentrations of attached peptides are determined based on the geometric area (0.33 cm^2) of flat gold disk electrodes.

3. Results and Discussion

3.1. Conformation analysis of peptides

The geometry of peptides **1**-**4** was confirmed as 3_{10}-helical by ^1H NMR spectroscopy. Specifically, strong N*H* (*i*) to N*H* (*i*+1) ROESY correlations were found for these peptides, together with Cα*H* (*i*) to N*H* (*i*+1) and medium range Cα*H* (*i*) to N*H* (*i*+2) correlations. A Cα*H* (*i*) to N*H* (*i*+2) cross peak is only possible for a 3_{10}-helix [45], as the distance between these two hydrogen atoms is in the order of 3.5 Å, whereas in an α-helix the distance between Cα*H* (*i*) to N*H* (*i*+2) atoms is approximately 4.5 Å, and near the limit of detection [46]. An absence of Cα*H* (*i*) to N*H* (*i*+4) correlations was noted for all peptides, thus excluding the

possibility of an α-helical structure, which is characterized by (*i* to *i*+4) hydrogen bonds [47]. Strong correlations were also evident for CβH_2 (*i*) and N*H* (*i*) in peptides **1** and **3** [23]. A strong negative minimum near 202 nm, with a far weaker minimum at approximately 232 nm was observed in a representative CD spectrum of N-Boc protected peptide **1** (as shown in Fig.4a) which further supports a 3_{10}-helical conformation [36, 48]. Hence the cumulative ^{1}H NMR and CD data confirm the presence of 3_{10}-helical structures for each of peptides **1**-**4.** Moreover, the C-terminal ferrocene moieties and the side-bridge constraints do not impinge on the backbone helicity. The conformations of peptides **5-8** were confirmed as β-strand by a combination of ^{1}H NMR and IR spectroscopy. Cα*H* (*i*) to N*H* (*i*+1) and Cβ*H* (*i*) to N*H* (*i*+1) ROESY correlations were found for all four peptides (as shown in Fig. 4b and 4c), indicative of a β-strand geometry [49]. Furthermore, ^{1}H NMR $J_{NHC\alpha H}$ coupling constants [49] of 8-10 Hz were observed for these peptides. Amide I and II bands are used extensively in IR spectroscopy for peptide/protein structural determination. Typically for a β-strand conformation, a strong band (Amide I) is evident between 1612 and 1640 cm^{-1}, while another strong band (Amide II) is located between 1510 and 1530 cm^{-1}. Peptides **5**-**8** fall within this category, confirming their β-strand structure, with a representative spectrum (peptide **8**) shown in Fig. 4d. Amide A (N-H stretching) frequencies between 3277 and 3293 cm^{-1} were also observed in the IR spectra of peptides **5**-**8**, providing further evidence of structure [50].

[Figure 4]

The lowest energy conformers for the *N*-Boc protected analogues of **1**-**8** were determined by molecular modelling in order to further define the backbone geometries. The resulting

models for the *N*-protected helical analogues of **1**-**4** (see Fig. 5) indicate that the backbone lengths (from first to last carbonyl carbons) are very similar (11.94, 12.02, 11.91, 11.91 Å for the *N*-Boc protected analogues of **1**-**4** respectively) differing by no more than 0.11 Å. The mean intramolecular hydrogen bond lengths are 2.16, 2.12, 2.10 and 2.13 Å for *N*-Boc protected analogues of **1**-**4** respectively, with a variation of less than 0.06 Å. The calculated hydrogen bond lengths are in accordance with similar 3_{10}-helical structures reported elsewhere [23, 25, 36]. The most significant difference in the intramolecular hydrogen bond lengths for each of the helical peptides is only 0.15 Å, between residues 2 and 5 in peptides **3** and **4**, which correspond to the *i* and *i*+3 positions of the side-bridge constraint. Table 1 lists dihedral angles for all residues in the lowest energy conformers for *N*-Boc protected helical peptides **1**-**4**. The average dihedral angles for residues 1-6 in each of the *N*-Boc protected analogues, deviate from an ideal 3_{10}-helix by no more than 3.6° and 5.9° for Φ and ψ respectively. All these geometric parameters are in good agreement with similar 3_{10}-helical structures [23, 25, 36]. The calculated lowest energy conformers for the *N*-Boc protected β-strand analogues of **5-8** (see Fig. 6) indicate that the backbone length (from first to last carbonyl carbons) are once again very similar (10.38, 10.61, 10.67 and 10.97 Å for the *N*-Boc protected analogues of **5**-**8** respectively, as shown in Table 2). The largest variation in backbone length is 0.59 Å, between the linear analogue of **5** and the unsaturated analogue of **8**. All other dimensions critical to the characterization of a β-strand conformation, such as N*H* (*i*) to N*H* (*i*+1), Cα*H* (*i*) to N*H* (*i*+1) and CβH_2 (*i*) to N*H* (*i*+1) distances as detailed in Table 2 are in accordance with literature values [51].

[Figure 5]

Table 1. Dihedral angles for all residues in the lowest energy conformers for *N*-Boc protected helical peptides **1**-**4**.

Residue	Boc-protected **1**		Boc-protected **2**		Boc-protected **3**		Boc-protected **4**	
	Φ	ψ	Φ	ψ	Φ	ψ	Φ	ψ
1	-63.47°	-30.13°	-62.66°	-30.73°	-65.15°	-27.91°	-64.78°	-28.06°
2	-54.84°	-29.06°	-64.79°	-16.92°	-61.75°	-18.79°	-54.91°	-28.35°
3	-54.16°	-32.47°	-51.78°	-29.08°	-50.60°	-30.48°	-54.25°	-27.51°
4	-54.95°	-33.48°	-54.08°	-28.25°	-52.94°	-30.80°	-53.96°	-28.36°
5	-74.11°	-6.61°	-54.47°	-31.13°	-67.197°	-13.26°	-53.76°	-31.59°
6	-65.89°	-26.01°	-66.48°	-20.92°	-66.12°	-23.38°	-66.64°	-20.29°

A combination of the molecular modelling studies and spectroscopic characterisations (including ^{1}H NMR, IR and CD data) demonstrates that peptides **1-4** share remarkably similar 3_{10}-helical conformations, while peptides **5-8** exhibit a common β-strand geometry. Thus the prominent structural differences between each of these peptides and hence the analogues, are simply the presence (or absence) of the side-bridge constraint, and the associated effect that this has on backbone rigidity as discussed below.

[Figure 6]

Table 2. Structural data for peptides **5**-**8**, with comparison to optimal β-strand values.

	Boc-protected **5**	Boc-protected **6**	Boc-protected **7**	Boc-protected **8**	Optimal β-strand conformation
Length (first to last carbonyl)	10.38	10.61	10.67	10.97	
Distance*	8.0	8.2	8.0	8.3	8.0 [51]
N-Leu to CO-Leu	2.3	2.4	2.4	2.4	2.5 [46]
NH to NH (Average)	4.3	4.3	4.3	4.3	4.3 [46]
αH to NH+1	2.3	2.5	2.2	2.2	2.2 [46]
βH_2 to NH+1	3.9	3.6	4.1	4.0	3.2 to 4.5 [46]

Note: * This distance is defined between the C atom (*i*) and N (*i*+3), which is indicative of an optimal extended β-strand. All distance values are reported in Å.

3.2. Electron transfer in peptides

Each of the peptides **1**-**8** was separately attached to vertically aligned single-walled carbon nanotube array/gold (SWCNTs/Au, as shown in Fig.3a) electrodes in order to study their electron transfer kinetics. Fig. 7 shows the cyclic voltammograms obtained for individual helical peptides immobilized electrodes immersed in 0.1 mol L^{-1} $TBAPF_6/CH_3CN$ solutions. These show a significant background current and a pair of redox peaks. Due to the rough

surface of SWCNTs/Au (Fig. 3), a large background current is always observed as shown in Fig. 7b [42, 52]. After background subtraction, the characteristic of a one-electron oxidation / reduction reaction (Fc^+/Fc) comes to the fore. The surface concentrations of the peptides were determined, by integrating faradaic current peak areas, to be 3.76×10^{-10} mol cm^{-2} for **1**, 2.52×10^{-10} mol cm^{-2} for **2**, 4.37×10^{-10} mol cm^{-2} for **3**, and 4.02×10^{-10} mol cm^{-2} for **4** (see Table 3). These surface concentrations are comparable to other carbon nanotube electrode studies [11, 42].

[Figure 7]

Table 3. Electron transfer rate constants (k_{et}), surface concentrations and formal potentials (E_o) for the helical peptides **1**-**4**.

Peptide	Surface concentration ($\times10^{-10}$ mole.cm^{-2})	E_o (V *vs* AgCl/Ag)	k_{et} * / s^{-1}
1	3.76 ± 0.35	0.853	28.1 ± 3.6
2	2.52 ± 0.18	0.371	117.3 ± 9.9
3	4.37 ± 0.43	0.844	17.5 ± 1.5
4	4.02 ± 0.41	0.380	260.4 ± 25.3

Note: * Standard deviation with electrochemical measurements on three electrodes.

These four hexapeptides share a common 3_{10}-helical conformation, while peptides **1** and **3** were further constrained into this conformation via a triazole-containing linker introduced by Huisgen cycloaddition, and an alkene-containing linker introduced by ring-closing metathesis, respectively. The constrained peptides (**1** and **3**) and their linear analogues (**2** and **4**) exhibited considerably different formal potentials and electron transfer rate

constants. Specifically, the formal potentials (E_o) and apparent electron transfer rate constants (k_{et}) fall into two distinct groups. This is clearly evidenced in the plot of peak potential versus ln(scan rate) as shown in Fig.7d, with a broad range of scan rate employed. The linear analogues displayed low formal potentials and high electron transfer rate constants, estimated to be 0.371 V and 117.3 s^{-1} for **2**, 0.380 V and 260.4 s^{-1} for **4** (as detailed in Table 3), using Laviron's formalism [53]. The observed formal potentials for these linear peptides are similar to the formal potentials reported for other ferrocene-derivatized linear peptides attached to a gold surface, without carbon nanotubes [13, 27]. This further supports previous observations that carbon nanotubes have no significant effect on the electron transfer rate-limiting step [11, 42]. Contrary to this, the constrained peptides exhibited high formal potentials and low electron transfer rate constants, estimated to be 0.853 V and 28.1 s^{-1} for **1**, 0.844 V and 17.5 s^{-1} for **3**. Peptide **1**, with a triazole-containing side-bridge, shows a significant formal potential shift to the positive of approximately 480 mV, in comparison to the linear peptide **2**. Also a dramatic shift to the positive in the formal potential of the cyclic peptide **3**, constrained by an alkene-containing tether, was also observed (464 mV) compared with that of the linear **4**. Such remarkable formal potential shifts are significantly higher compared to other conformation-dependent structures, such as cis-trans cyclohexasilanes (110 mV) [54]. Thus oxidation/reduction of the redox-active ferrocene moieties in the constrained peptides is energetically much less favourable than those in the linear analogues. Our experimental results also reveal a significant decrease in the electron transfer rate constant upon the introduction of the constraints. The data from these compounds reveals an electron transfer rate constant for the constrained peptide **1** of 28.1 s^{-1}, 4-fold lower than that of the linear counterpart **2**. Furthermore, an electron transfer rate constant for the constrained peptide **3** is estimated to be 17.5 s^{-1}, a remarkable 15-fold

lower than that of the linear counterpart **4**. Previous studies have shown that electron transfer rate constants in peptides can vary greatly [11, 13, 55], but not to such an extent as reported here. The vast formal potential shifts and electron transfer rate constant drops in these peptides provide two distinct states (i.e. on/off). These states, brought about through side-bridge gating, afford a sizeable differential which is ideal for the design of molecular switches.

Theoretical calculations would provide further insight into the intramolecular electron transfer dynamics. Since single-step superexchange and multistep tunneling are widely accepted charge-transport mechanisms in peptides [11, 27, 56], we compared reorganisation energies for multiple sequential electron transfer steps along the helical peptide backbones. Peptides **9** and **10** were chosen for this study since they contain the same sequence as **1** and **2**, but with ferrocene units at both termini to act as both a donor and acceptor. Diabatic states were constructed by individually localizing an overall charge of 1 on each of the ferrocene units and amino acids, as shown in Fig. 8. The constrained peptide and its linear analogue show comparable reorganisation energies for all sequential tunnelling steps, except those providing a linking site for the side-bridge (i.e. S3). The reorganisation energies for the forward and backward electron steps from S3 in **9** are much higher than the corresponding steps in **10** (see Table 4). The introduction of the side-bridge gives rise to a significant increase in reorganisation energy, in the range of 3.14 – 6.97 $kcal.mol^{-1}$. The higher reorganisation energy barrier in peptide **9** is a direct result of the side-bridge constraint, thus further supporting our experimental results. Additionally, Maran[30] and Santi[31] showed that the direction of the associated dipole moment in a 3_{10}-helix could strongly influence the formal potentials. In particular, it is expected to stabilize the

ferrocenyl group if the negative end of the dipole is adjacent to the ferrocene moiety. This would also push the oxidation of the ferrocene moiety toward more positive potentials.

Table 4. Computed reorganisation energies for sequential tunnelling steps in the two model peptides **9** and **10.**

Sequential steps	Peptide **9** (kcal.mol^{-1})	Peptide **10** (kcal.mol^{-1})	Difference (kcal.mol^{-1})
S2 → S3	28.99	24.09	4.90
S3 → S2	30.62	24.57	6.05
S3 → S4	25.41	22.27	3.14
S4 → S3	30.68	23.71	6.97

[Figure 9]

Table 5. Electron transfer rate constants (k_{et}), surface concentrations and formal potentials (E_o) for the β-strand peptides **5**-**8**.

Peptide	Surface concentration (×10^{-10} mole.cm^{-2})	E_o (V *vs* AgCl/Ag)	k_{et}^* (s^{-1})
5	5.86 ± 0.54	0.825	22.5 ± 2.1
6	2.73 ± 0.26	0.349	223.2 ± 23.2
7	9.21 ± 0.89	0.676	11.7 ± 1.2
8	5.56 ± 0.31	0.408	421.4 ± 41.5

Note: * Standard deviation with electrochemical measurements on three electrodes.

Fig. 9 shows the cyclic voltammograms obtained for the β-strand peptides immersed in 0.1 mol L^{-1} $TBAPF_6/CH_3CN$ solutions. Similarly, these show a pair of redox peaks, characteristic of a one-electron oxidation / reduction reaction (Fc^+/Fc). Surface concentrations for the β-strand peptides **5**-**8** are comparable to those of the helical peptides. The values were determined to be 5.86×10^{-10} mol cm^{-2} for **5**, 2.73×10^{-10} mol cm^{-2} for **6**, 9.21×10^{-10} mol cm^{-2} for **7**, and 5.56×10^{-10} mol cm^{-2} for **8** (see Table 5). The observed formal potentials (E_o) and apparent electron transfer rate constants (k_{et}) were estimated from the plot of peak potential versus ln(scan rate) as shown in Fig.9b and Table 5. These parameters also fall into two definitive groups. The linear analogues displayed low formal potentials and high electron transfer rate constants, estimated to be 0.349 V, 223.2 s^{-1} for **6**, and, 0.408 V, 421.4 s^{-1} for **8** (as detailed in Table 5), whereas the constrained peptides exhibited high formal potentials and low electron transfer rate constants, estimated to be 0.825 V, 22.5 s^{-1} for **5**, and, 0.844 V, 11.7 s^{-1} for **7**. These four tripeptides share a common β-strand conformation, while peptides **5** and **7** were further constrained into this conformation by a triazole-containing and an alkene-containing linker respectively. Peptide **5**, with the triazole-containing constraint shows a significant formal potential shift to the positive of approximately 476 mV, in comparison to the linear peptide **6**. A dramatic shift to the positive in the formal potential of the constrained peptide **7**, with an alkene-containing side-bridge, was also observed (268 mV) compared to that of the linear counterpart **8**. The experimental data on these β-strand compounds also reveal an electron transfer rate constant for the constrained peptide **5** of 22.5 s^{-1}, 10-fold lower than that of the linear peptide **6**. Furthermore, an electron transfer rate constant for the constrained peptide **7** is estimated to be 11.7 s^{-1}, a remarkable 36-fold lower than that of the linear peptide **8**. This clearly demonstrates that an increase in backbone rigidity, imparted by the side-chain

constraints of **5** and **7**, significantly hinders oxidation/reduction of the redox-active ferrocene moiety.

Our results demonstrate an important link between backbone rigidity and the efficiency of electron transfer in peptides. They also further extend the generality of this effect, irrespective of the backbone conformation (either helical or β-strand) and the nature of the side-bridge constraint (either a triazole-containing or an alkene-containing linker). It is believed that side-bridge stapling creates an additional reorganisation energy barrier that impedes electron transfer within the peptide, in turn decreasing the charge transfer rate [25, 26]. Hence reducing the backbone flexibility within a helical peptide, through the introduction of a constraint, lowers the rate of electron transfer by restricting the precise torsional motions that lead to facile intramolecular electron transfer along the backbone. Thus side-bridge stapling provides a unique approach to manipulate energy barriers and conductance in peptides.

3.3. Influence of side-chain on electron transfer

A comparison of the data for the two linear hexapeptides (**2** and **4**) provides a measure of the influence of the electron rich alkene side-chains on the rate of electron transfer. These two peptides share a common 3_{10}-helical conformation and contain the same number of Aib residues, while they differ only in the structure of the side-chain, as shown in Fig. 1. Peptide **2** comprises a triazole-containing side-chain, while an alkene-containing side-chain is situated at the same location in peptide **4**. The observed electron transfer rate constant for **4** was 260.4 s^{-1} (see Table 4), 2-fold higher than that for **2**. This observation is reinforced for the two β-strand linear peptides (**6** and **8**). Similarly, these two tripeptides differ only in

their side-chains, as shown in Fig. 2, with a triazole-containing side-chain incorporated into **6** and an alkene-containing side-chain in **8**. The observed electron transfer rate constant for **8** was 421.4 s^{-1} (see Table 5), 2-fold higher than that for **6**. This clearly demonstrates the ability of the electron-rich alkene and phenol groups to facilitate electron transfer through the peptide by acting as a 'stepping stone'.

It is important to investigate the experimental data for the two constrained hexapeptides (**1** and **3**) since they do not seem to follow the tendency evident in the linear peptides. These two constrained hexapeptides differ in the covalent tether linking their *i* and *i*+3 residues. Peptide **1** contains a triazole-containing side-bridge, forming a 19-member macrocyclic ring, while peptide **3** possesses an alkene-containing side-bridge, generating a smaller and potentially tighter 18-member macrocyclic ring. The alkene-containing side-bridge in **3** provides a potential 'stepping stone' for electron transfer, while the smaller macrocyclic ring introduces additional rigidity to the backbone of the peptide in comparison to that in peptide **1.** These effects are opposing, with the first expected to increase the electron transfer rate and the second to decrease it. Interestingly, peptide **3** gave an approximate 160% decrease in the electron transfer rate relative to **1**, which clearly shows that an increase in backbone rigidity in helical peptides decreases the efficiency of electron transfer. Furthermore, the β-strand peptide **5**, comprising a triazole-containing side-bridge linking its *i* to *i*+2 residues, forms a 16-member macrocyclic ring, while peptide **7** has an alkene-containing side-bridge, generating a 17-member macrocyclic ring. Curiously, peptide **7** gave an approximate 2-fold decrease in the electron transfer rate relative to **5**, with values of 11.7 s^{-1} and 22.5 s^{-1} respectively (see Tables 5). The planar nature of the electron-rich alkene and phenol components in **7** is able to influence both the backbone rigidity and potentially

the electronic properties with its inclusion in the ring**.** However, the results show that the effect of backbone rigidity, arising from the alkene and phenol components in **7**, appears to be the dominant factor in this case. Manipulating the chemical composition and backbone rigidity of peptides provides a new means to fine tune electron transfer kinetics, which represents an important step towards their implementation into molecular electronic assemblies. Such structurally diverse peptides with controllable electronic functions open new avenues in the design and fabrication of efficient components for molecular-based electronic devices.

4. Conclusions

Electrochemical studies are reported on a series of peptides **1**-**8** to determine the influence of different side-chains and backbone rigidity on electron transfer. Peptides **1**-**4** contain Aib residues that constrain the backbones into a well-defined 3_{10}-helix. Peptide **2** comprises a triazole-containing side-chain, while an alkene-containing side-chain is located at the same position for **4**. Peptides **1** and **3** were further constrained into a 3_{10}-helix with a side chain tether, resulting in additional conformational rigidity in their backbones. Peptides **5**-**8** share a common β-strand conformation, with **6** comprising a triazole-containing side-chain, and **8** possessing an alkene-containing side-chain at the same location. The backbones of peptides **5** and **7** were further constrained into a β-strand conformation with a triazole-containing and an alkene-containing linker respectively. Electrochemical studies revealed a direct link between backbone rigidity and the efficiency of electron transfer, irrespective of the backbone conformation (either helical or β-strand) and the nature of the side-bridge constraint (either a triazole-containing or an alkene-containing linker). The formal potentials (E_o) and apparent electron transfer rate constants (k_{et}) fall into two distinct groups. One

group represented by the linear peptides displayed low formal potentials and high electron transfer rate constants, whereas the other containing the constrained peptides, exhibited high formal potentials and low electron transfer rate constants. Specifically, all constrained peptides (**1**, **3**, **5** and **7**) recorded a significant formal potential shift to the positive (482, 464, 476 and 268 mV, respectively), and a substantial decrease in the electron transfer rate constant (76%, 93%, 90% and 97%), compared to their unconstrained, linearcounterparts **2**, **4**, **6** and **8**. These vast formal potential shifts and electron transfer rate constant drops represent two distinct states (i.e. on/off) with a large differential, which is ideal for the design of molecular switches. These findings, brought about through side-bridge gating, provide a new approach to fine tune the electronic properties of peptides through chemical modification of the backbone to increase/decrease rigidity, and through the inclusion of electron rich side-chains.

Acknowledgements

We acknowledge the Australian Research Council (ARC) Centre of Excellence for Nanoscale BioPhotonics (CNBP) for the financial support of this work. J.Y. acknowledges the Faculty of Sciences, the University of Adelaide for an international travel grant, enabling him to present this work at the 66th ISE Annual Meeting. We also acknowledge the Australian National Fabrication Facility for providing the analytical facilities. The computational aspects of this work were supported by an award under the National Computational Merit Allocation Scheme (NCMAS) for JY on the National Computing Infrastructure (NCI) National Facility at the Australian National University.

References

[1] A. Aviram, M.A. Ratner, Molecular rectifiers, Chemical Physics Letters, 29 (1974) 277-283.

[2] M. Ratner, A brief history of molecular electronics, Nature Nanotechnology, 8 (2013) 378-381.

[3] J.L. Zhang, J.Q. Zhong, J.D. Lin, W.P. Hu, K. Wu, G.Q. Xu, A.T.S. Wee, W. Chen, Towards single molecule switches, Chemical Society Reviews, 44 (2015) 2998-3022.

[4] M.E. Carbone, R. Ciriello, S. Granafei, A. Guerrieri, A.M. Salvi, EQCM and XPS investigations on the redox switching of conducting poly(o-aminophenol) films electrosynthesized onto Pt substrates, Electrochimica Acta, 176 (2015) 926-940.

[5] L.C.T. Shoute, Y. Wu, R.L. McCreery, Direct spectroscopic monitoring of conductance switching in polythiophene memory devices, Electrochimica Acta, 110 (2013) 437-445.

[6] G. Ybarra, C. Moina, M.I. Florit, D. Posadas, Current rectification by mediating electroactive polymers, Electrochimica Acta, 53 (2008) 3955-3959.

[7] N. Amdursky, D. Marchak, L. Sepunaru, I. Pecht, M. Sheves, D. Cahen, Electronic Transport via Proteins, Advanced Materials, 26 (2014) 7142-7161.

[8] R.E. Blankenship, Early Evolution of Photosynthesis, Plant Physiology, 154 (2010) 434-438.

[9] A. Shah, B. Adhikari, S. Martic, A. Munir, S. Shahzad, K. Ahmad, H.-B. Kraatz, Electron transfer in peptides, Chemical Society Reviews, (2015) DOI: 10.1039/C1034CS00297K.

[10] F. Maran, C. Toniolo, Peptide and protein mediated electron and energy transfer, Biopolymers, 100 (2013) iii-iv.

[11] J. Yu, O. Zvarec, D.M. Huang, M.A. Bissett, D.B. Scanlon, J.G. Shapter, A.D. Abell, Electron Transfer through α-Peptides Attached to Vertically Aligned Carbon Nanotube Arrays: A Mechanistic Transition, Chemical Communications, 48 (2012) 1132–1134.

[12] S. Sek, A. Sepiol, A. Tolak, A. Misicka, R. Bilewicz, Distance Dependence of the Electron Transfer Rate through Oligoglycine Spacers Introduced into Self-Assembled Monolayers, The Journal of Physical Chemistry B, 108 (2004) 8102-8105.

[13] Y. Arikuma, H. Nakayama, T. Morita, S. Kimura, Electron Hopping over 100 angstrom Along an alpha Helix, Angewandte Chemie-International Edition, 49 (2010) 1800.

[14] E. Gatto, M. Venanzi, Self-assembled monolayers formed by helical peptide building blocks: a new tool for bioinspired nanotechnology, Polymer Journal, 45 (2013) 468-480.

[15] J.X. Yu, S. Mathew, B.S. Flavel, M.R. Johnston, J.G. Shapter, Ruthenium porphyrin functionalized single-walled carbon nanotube arrays - A step toward light harvesting antenna and multibit information storage, Journal of the American Chemical Society, 130 (2008) 8788.

[16] J. Juhaniewicz, J. Pawlowski, S. Sek, Electron Transport Mediated by Peptides Immobilized on Surfaces, Israel Journal of Chemistry, 55 (2015) 645-660.

[17] G. Maruccio, Molecular electronics: Protein transistors strike gold, Nature Nanotechnology, 7 (2012) 147-148.

[18] Y. Mou, J.-Y. Yu, T.M. Wannier, C.-L. Guo, S.L. Mayo, Computational design of co-assembling protein-DNA nanowires, Nature, 525 (2015) 230-233.

[19] D.W.P.M. Lowik, E.H.P. Leunissen, M. van den Heuvel, M.B. Hansen, J.C.M. van Hest, Stimulus responsive peptide based materials, Chemical Society Reviews, 39 (2010) 3394-3412.

[20] T. Kumeria, J. Yu, M. Alsawat, M.D. Kurkuri, A. Santos, A.D. Abell, D. Losic, Photoswitchable Membranes Based on Peptide-Modified Nanoporous Anodic Alumina: Toward Smart Membranes for On-Demand Molecular Transport, Advanced Materials, 27 (2015) 3019-3024.

[21] S. Yasutomi, T. Morita, Y. Imanishi, S. Kimura, A molecular photodiode system that can switch photocurrent direction, Science, 304 (2004) 1944-1947.

[22] K.V. Korpany, P. Langat, D.M. Kim, N. Edelman, D.R. Cooper, J. Nadeau, A.S. Blum, Conductance Switching in the Photoswitchable Protein Dronpa, Journal of the American Chemical Society, 134 (2012) 16119-16122.

[23] O. Jacobsen, H. Maekawa, N.H. Ge, C.H. Gorbitz, P. Rongved, O.P. Ottersen, M. Amiry-Moghaddam, J. Klaveness, Stapling of a 3(10)-Helix with Click Chemistry, Journal of Organic Chemistry, 76 (2011) 1228.

[24] D.S. Pedersen, A. Abell, 1,2,3-Triazoles in Peptidomimetic Chemistry, European Journal of Organic Chemistry, 2011 (2011) 2399-2411.

[25] J. Yu, J.R. Horsley, K.E. Moore, J.G. Shapter, A.D. Abell, The Effect of a Macrocyclic Constraint on Electron Transfer in Helical Peptides: A Step Towards Tunable Molecular Wires Chemical Communications, 50 (2014) 1652.

[26] J.R. Horsley, J. Yu, K.E. Moore, J.G. Shapter, A.D. Abell, Unraveling the Interplay of Backbone Rigidity and Electron Rich Side-Chains on Electron Transfer in Peptides: The Realization of Tunable Molecular Wires, Journal of the American Chemical Society, 136 (2014) 12479-12488.

[27] H.S. Mandal, H.-B. Kraatz, Electron Transfer Mechanism in Helical Peptides, The Journal of Physical Chemistry Letters, 3 (2012) 709–713.

[28] S. Antonello, F. Formaggio, A. Moretto, C. Toniolo, F. Maran, Anomalous distance dependence of electron transfer across peptide bridges, Journal of the American Chemical Society, 125 (2003) 2874.

[29] F. Polo, S. Antonello, F. Formaggio, C. Toniolo, F. Maran, Evidence against the hopping mechanism as an important electron transfer pathway for conformationally constrained oligopeptides, Journal of the American Chemical Society, 127 (2005) 492.

[30] L. Garbuio, S. Antonello, I. Guryanov, Y. Li, M. Ruzzi, N.J. Turro, F. Maran, Effect of Orientation of the Peptide-Bridge Dipole Moment on the Properties of Fullerene-Peptide-Radical Systems, Journal of the American Chemical Society, 134 (2012) 10628-10637.

[31] A. Donoli, V. Marcuzzo, A. Moretto, C. Toniolo, R. Cardena, A. Bisello, S. Santi, Charge Mapping in 3(10)-Helical Peptide Chains by Oxidation of the Terminal Ferrocenyl Group, Organic Letters, 13 (2011) 1282.

[32] F. Formaggio, A. Moretto, S. Antonello, F. Maran, C. Toniolo, Role of intramolecular H-bonds on the electron-transfer rate in structurally defined peptides, Biopolymers, 71 (2003) P069.

[33] J. Yu, J.R. Horsley, A.D. Abell, The Influence of Secondary Structure on Electron Transfer in Peptides, Australian Journal of Chemistry, 66 (2013) 848-851.

[34] M. Saviano, E. Benedetti, R.M. Vitale, B. Kaptein, Q.B. Broxterman, M. Crisma, F. Formaggio, C. Toniolo, X-ray diffraction analysis and conformational energy computations of beta-turn and 3(10)-helical peptides based on alpha-amino acids with an olefinic side chain. Implications for ring-closing metathesis, Macromolecules, 35 (2002) 4204-4209.

[35] D.F. Kennedy, M. Crisma, C. Toniolo, D. Chapman, Studies of peptides forming 3(10)-helices and alpha-helices and beta-bend ribbon structures in organic solution and in model biomembranes by fourier-transform infrared-spectroscopy, Biochemistry, 30 (1991) 6541.

[36] A.K. Boal, I. Guryanov, A. Moretto, M. Crisma, E.L. Lanni, C. Toniolo, R.H. Grubbs, D.J. O'Leary, Facile and E-selective intramolecular ring-closing metathesis reactions in 3(10)-helical peptides: A 3D structural study, Journal of the American Chemical Society, 129 (2007) 6986-+.

[37] J.R. Horsley, J. Yu, A.D. Abell, The Correlation of Electrochemical Measurements and Molecular Junction Conductance Simulations in beta-Strand Peptides, Chemistry-a European Journal, 21 (2015) 5926-5933.

[38] N.A. Burton, M.J. Harrison, J.C. Hart, I.H. Hillier, D.W. Sheppard, Prediction of the mechanisms of enzyme-catalysed reactions using hybrid quantum mechanical molecular mechanical methods, Faraday Discussions, 110 (1998) 463-475.

[39] F.Z. Ding, H.B. Wang, Q. Wu, T. Van Voorhis, S.W. Chen, J.P. Konopelski, Computational Study of Bridge-Assisted Intervalence Electron Transfer, Journal of Physical Chemistry A, 114 (2010) 6039-6046.

[40] M. Valiev, E.J. Bylaska, N. Govind, K. Kowalski, T.P. Straatsma, H.J.J. van Dam, D. Wang, J. Nieplocha, E. Apra, T.L. Windus, W.A. de Jong, NWChem: a comprehensive and scalable open-source solution for large scale molecular simulations, Computer Physics Communications, 181 (2010) 1477.

[41] K.E. Moore, B.S. Flavel, J. Yu, A.D. Abell, J.G. Shapter, Increased redox-active peptide loading on carbon nanotube electrodes, Electrochimica Acta, 89 (2013) 206-211.

[42] J.J. Gooding, R. Wibowo, J.Q. Liu, W.R. Yang, D. Losic, S. Orbons, F.J. Mearns, J.G. Shapter, D.B. Hibbert, Protein electrochemistry using aligned carbon nanotube arrays, Journal of the American Chemical Society, 125 (2003) 9006-9007.

[43] P. Diao, Z.F. Liu, Vertically Aligned Single-Walled Carbon Nanotubes by Chemical Assembly - Methodology, Properties, and Applications, Advanced Materials, 22 (2010) 1430.

[44] D.H. Waldeck, D.E. Khoshtariya, Fundamental studies of long- and short-range electron exchange mechanisms between electrodes and proteins in 'Applications of Electrochemistry and Nanotechnology in Biology and Medicine I', edited by N.Eliaz., Modern Aspects of Electrochemistry 52 (2011) 105.

[45] H.E. Blackwell, J.D. Sadowsky, R.J. Howard, J.N. Sampson, J.A. Chao, W.E. Steinmetz, D.J. O'Leary, R.H. Grubbs, Ring-closing metathesis of olefinic peptides: Design, synthesis, and structural characterization of macrocyclic helical peptides, Journal of Organic Chemistry, 66 (2001) 5291-5302.

[46] K. Wüthrich, NMR of proteins and nucleic acids, Wiley1986.

[47] Z. Biron, S. Khare, A.O. Samson, Y. Hayek, F. Naider, J. Anglister, A monomeric 3(10)-helix is formed in water by a 13-residue peptide representing the neutralizing determinant of HIV-1 on gp41, Biochemistry, 41 (2002) 12687-12696.

[48] C. Toniolo, A. Polese, F. Formaggio, M. Crisma, J. Kamphuis, Circular dichroism spectrum of a peptide 3(10)-helix, Journal of the American Chemical Society, 118 (1996) 2744-2745.

[49] A.D. Pehere, A.D. Abell, New beta-Strand Templates Constrained by Huisgen Cycloaddition, Organic Letters, 14 (2012) 1330-1333.

[50] W. Zhuang, T. Hayashi, S. Mukamel, Coherent Multidimensional Vibrational Spectroscopy of Biomolecules: Concepts, Simulations, and Challenges, Angewandte Chemie-International Edition, 48 (2009) 3750-3781.

[51] P. Gillespie, J. Cicariello, G.L. Olson, Peptide Science, 43 (1997) 191.

[52] J. Yu, J.G. Shapter, M.R. Johnston, J.S. Quinton, J.J. Gooding, Electron-transfer Characteristics of Ferrocene Attached to SWCNT Arrays Directly Anchored to Silicon (100), Electrochimica Acta, 52 (2007) 6206.

[53] E. Laviron, The use of linear potential sweep voltammetry and of a.c. voltammetry for the study of the surface electrochemical reaction of strongly adsorbed systems and of redox modified electrodes, Journal of Electroanalytical Chemistry, 100 (1979) 263.

[54] R. Emanuelsson, H. Löfås, A. Wallner, D. Nauroozi, J. Baumgartner, C. Marschner, R. Ahuja, S. Ott, A. Grigoriev, H. Ottosson, Configuration- and Conformation-Dependent Electronic-Structure Variations in 1,4-Disubstituted Cyclohexanes Enabled by a Carbon-to-Silicon Exchange, Chemistry – A European Journal, 20 (2014) 9304-9311.

[55] M.M. Galka, H.B. Kraatz, Electron transfer studies on self-assembled monolayers of helical ferrocenoyl-oligoproline-cystamine bound to gold, Chemphyschem, 3 (2002) 356-+.

[56] M. Cordes, B. Giese, Electron transfer in peptides and proteins, Chemical Society Reviews, 38 (2009) 892-901.

Figure captions

Fig. 1. Structures of 3_{10}-helical peptides **1**-**4**, including cyclic peptides (**1** and **3**) and linear peptides (**2** and **4**).

Fig. 2. Structures of β-strand peptides **5-8**, including cyclic peptides (**5** and **7**) and linear peptides (**6** and **8**).

Fig. 3. (a) Typical AFM image of vertically aligned single-walled carbon nanotube array/gold (SWCNTs/Au) electrode. (b) Schematic of ferrocene-derivatised peptide immobilised SWCNTs/Au electrode.

Fig. 4. (a) CD spectrum representative of 3_{10}-helical peptide **1**. ^{1}H NMR ROSEY spectrum representative of β-strand peptide **5**, showing (b) Cα*H* (*i*) to N*H* (*i*+1) and (c) Cβ*H* (*i*) to N*H* (*i*+1) correlations. (d) IR spectrum representative of *N*-Boc protected β-strand peptide **8**.

Fig. 5. The lowest energy conformers from (a) to (d) for *N*-Boc protected 3_{10}-helicalanalogues of **1**-**4**respectively, optimized by the hybrid B3LYP method with 6-31G** basis set for all C, H, O, N atoms and Lanl2dz for Fe atom. (Inset: top view looking down helix.)

Fig. 6. The lowest energy conformers from (a) to (d) for *N*-Boc protected β-strand analogues of **5**-**8** respectively, optimized by the hybrid B3LYP method with 6-31G** basis set for all C, H, O, N atoms and Lanl2dz for Fe atom.

Fig. 7. (a) Cyclic voltammograms for helical peptides **1** (blue), **2** (red), **3** (black) and **4** (pink) immobilized on SWCNTs/Au electrodes taken at 5 V s^{-1} in 0.1 mol L^{-1} $TBAPF_6/CH_3CN$ solutions. (b) Typical cyclic voltammogram of SWCNTs/Au electrode taken at 5 V s^{-1} in 0.1 mol L^{-1} $TBAPF_6/CH_3CN$ solutions. (c) Background subtracted cyclic voltammogram (red solid)

from the original curve (blue solid) with the background current (dotted line). (d) Peak potential versus ln(scan rate) for peptides **1** (blue), **2** (red), **3** (black) and **4** (pink) after background current subtraction.

Fig. 8. Multiple sequential tunnelling steps in constrained peptide **9** (top) and unconstrained peptide **10** (bottom). Charge localisation fragments of the molecule involving the side bridge are indicated using two different colours in peptide **9**.

Fig. 9. (a) Cyclic voltammograms for helical peptides **5** (blue), **6** (red), **7** (black) and **8** (pink) immobilized on SWCNTs/Au electrodes taken at 5 V s^{-1} in 0.1 mol L^{-1} $TBAPF_6/CH_3CN$ solutions. (b) Peak potential versus ln(scan rate) for peptides **5** (blue), **6** (red), **7** (black) and **8** (pink) after background current subtraction.

Figure 01

Click here to download high resolution image

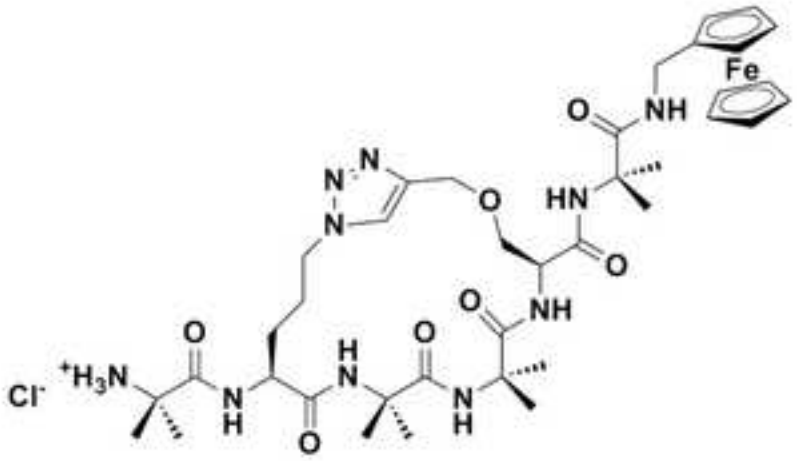

1

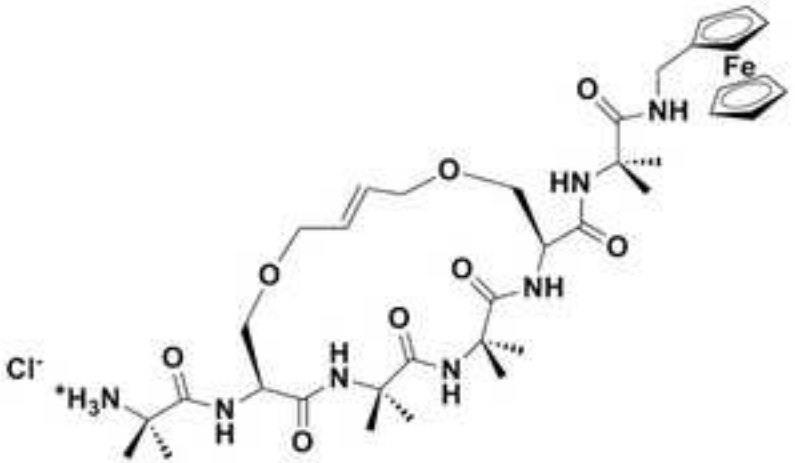

3

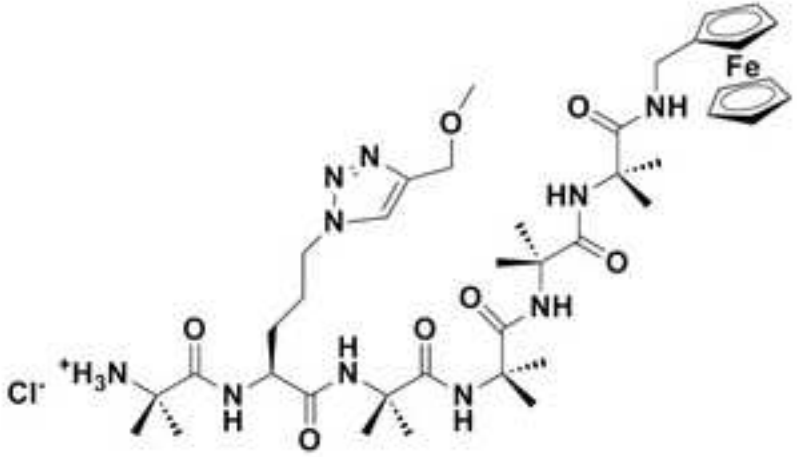

2

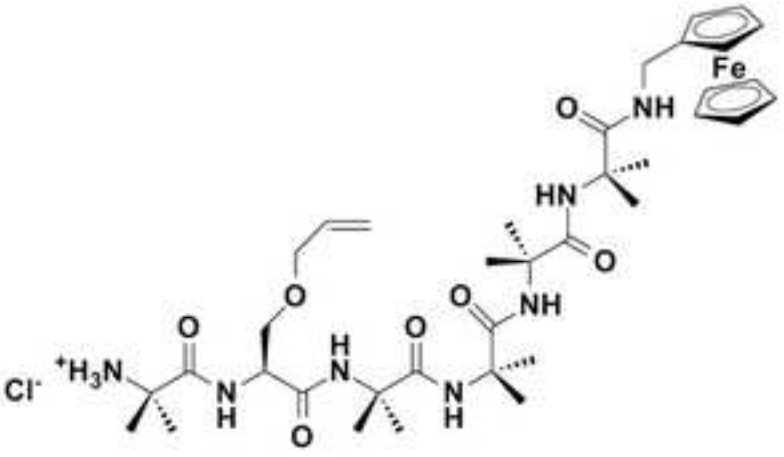

4

Figure 02

Click here to download high resolution image

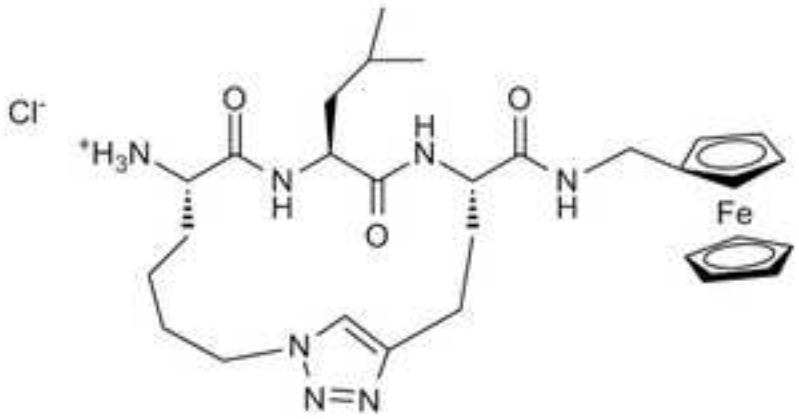

5

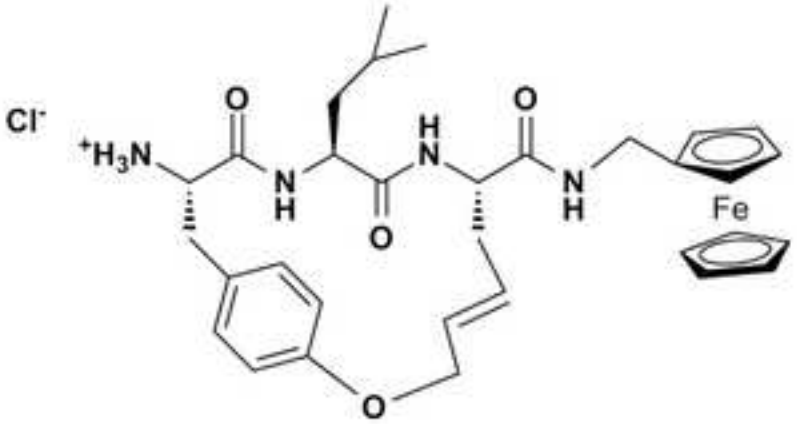

7

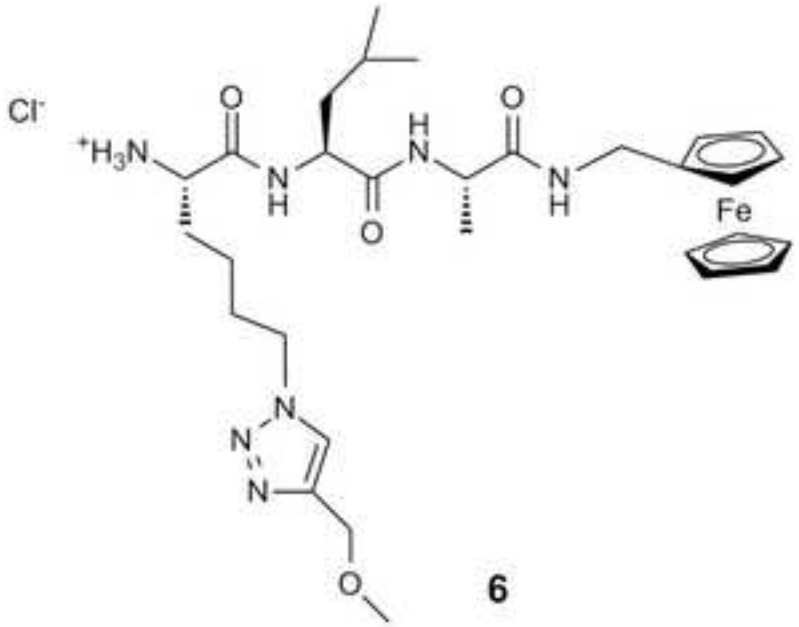

6

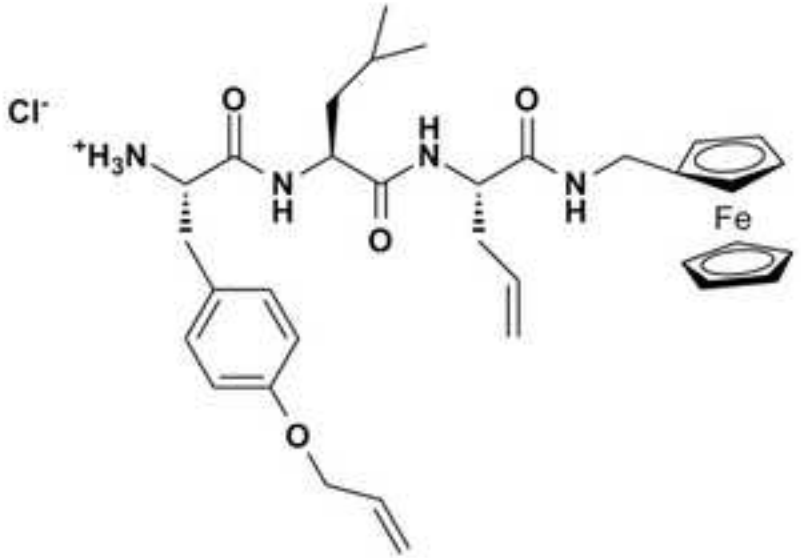

8

Figure 03(a)
Click here to download high resolution image

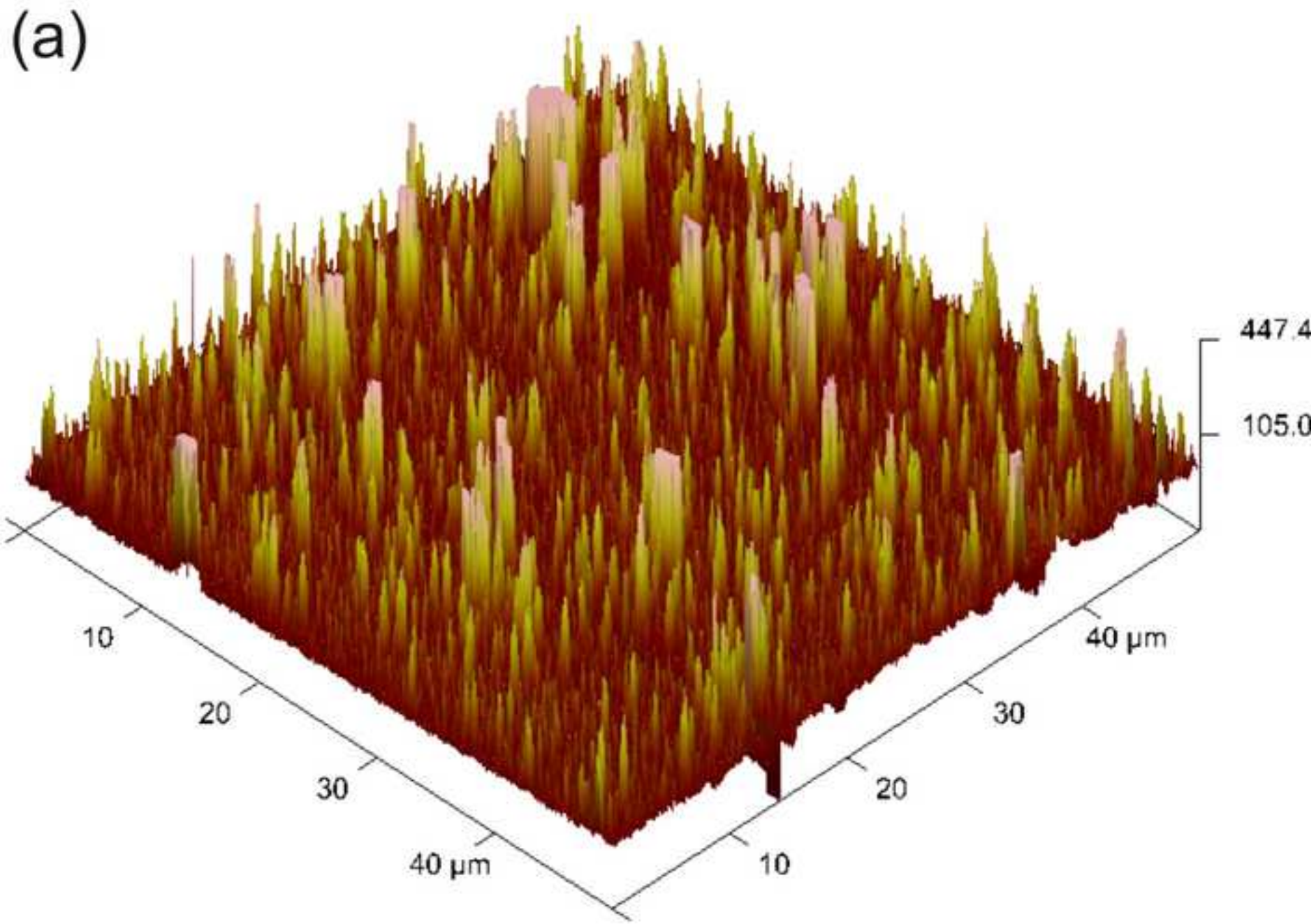

Figure 03(b)

Click here to download high resolution image

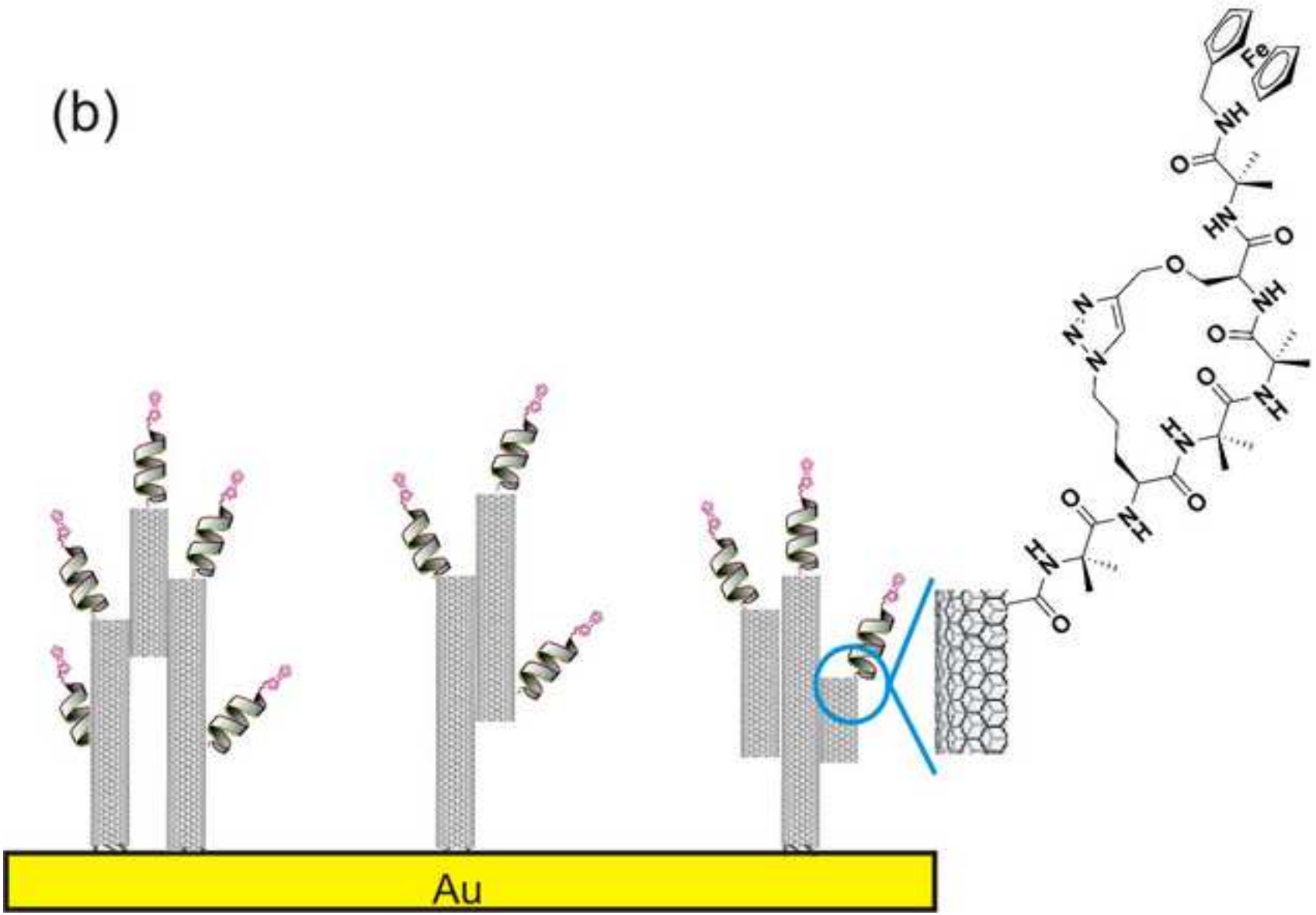

Figure 04(a)
Click here to download high resolution image

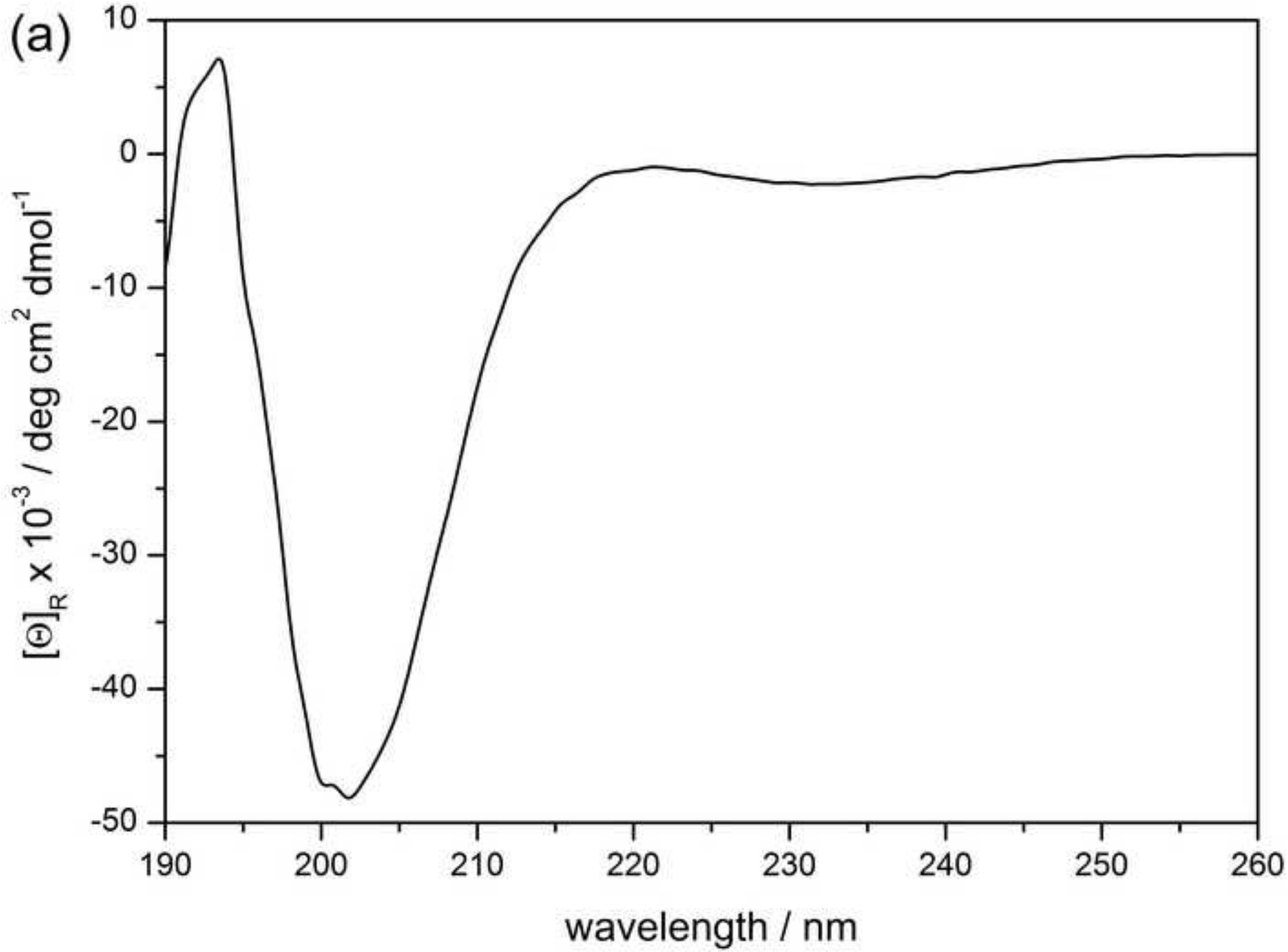

Figure 04(b)
Click here to download high resolution image

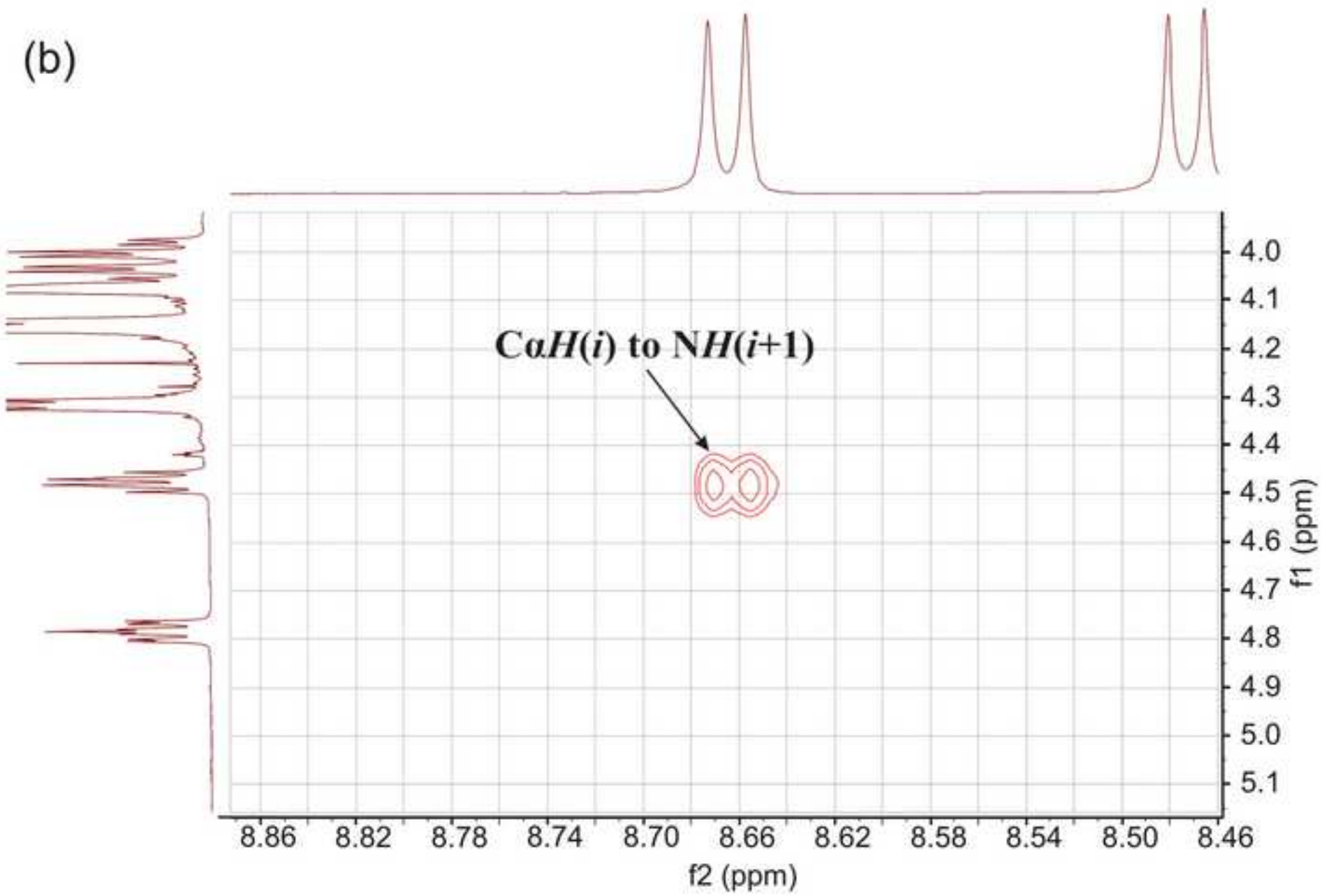

Figure 04(c)
Click here to download high resolution image

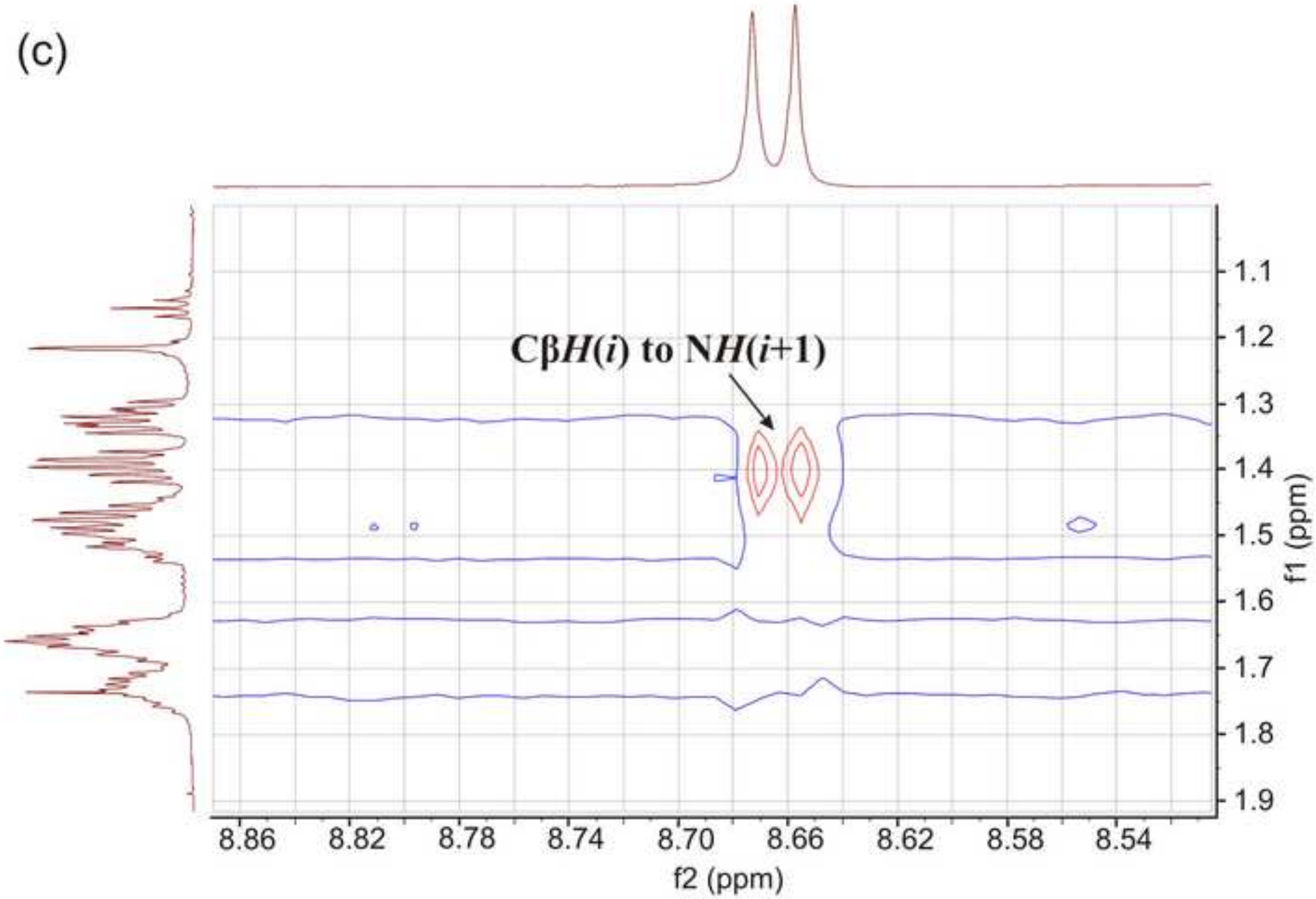

Figure 04(d)
Click here to download high resolution image

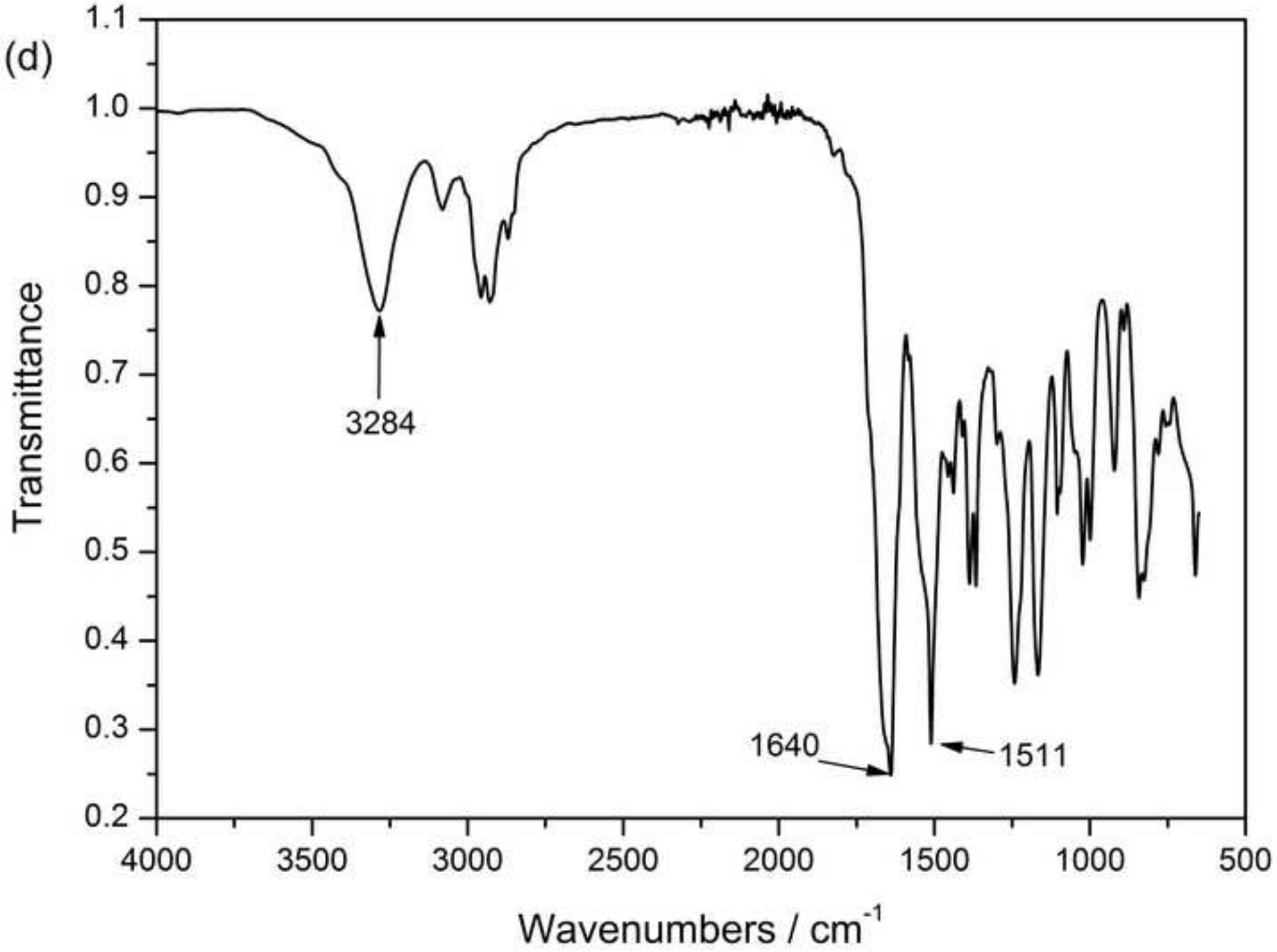

Figure 05

Click here to download high resolution image

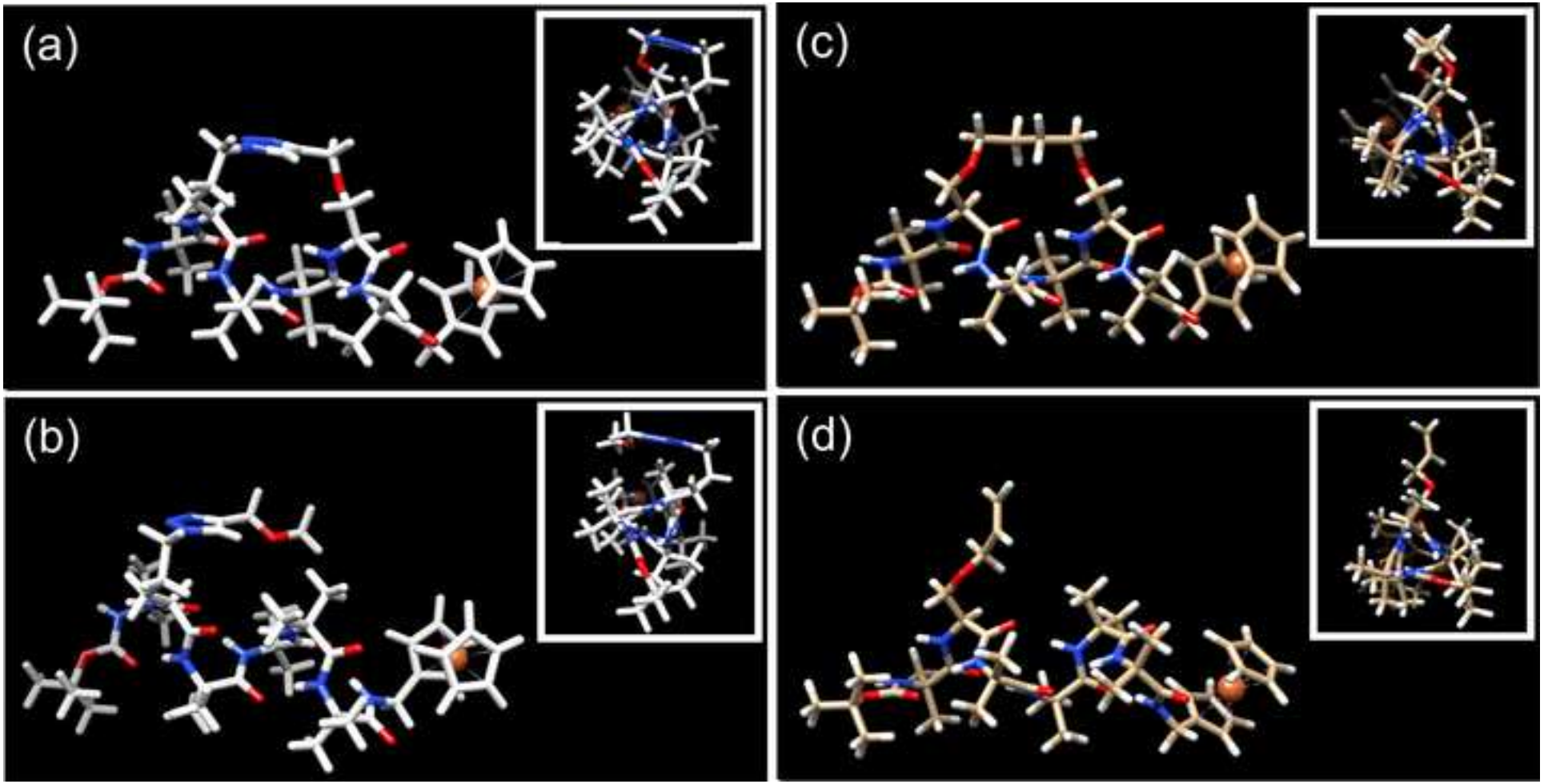

Figure 06

Click here to download high resolution image

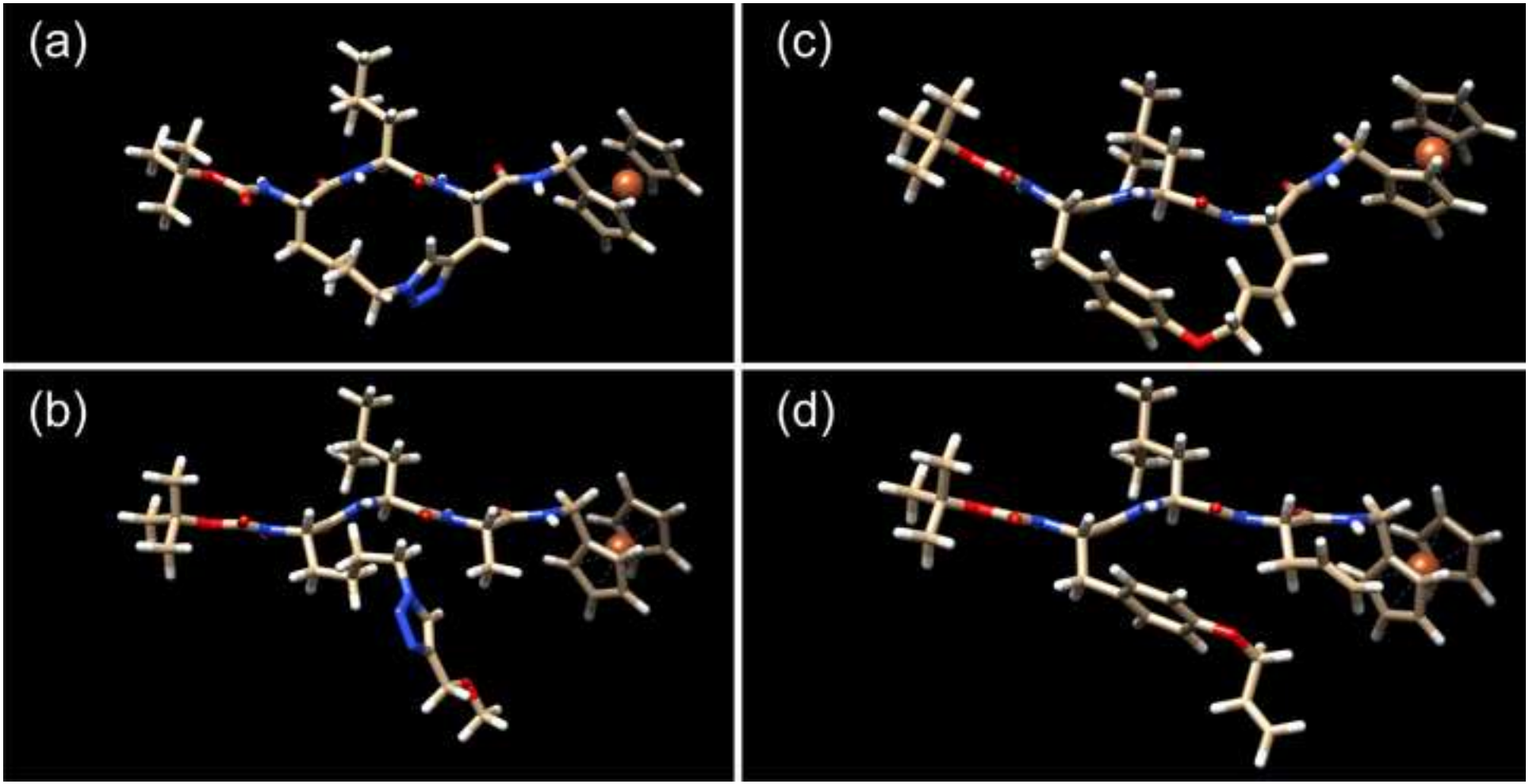

Figure 07(abc)
Click here to download high resolution image

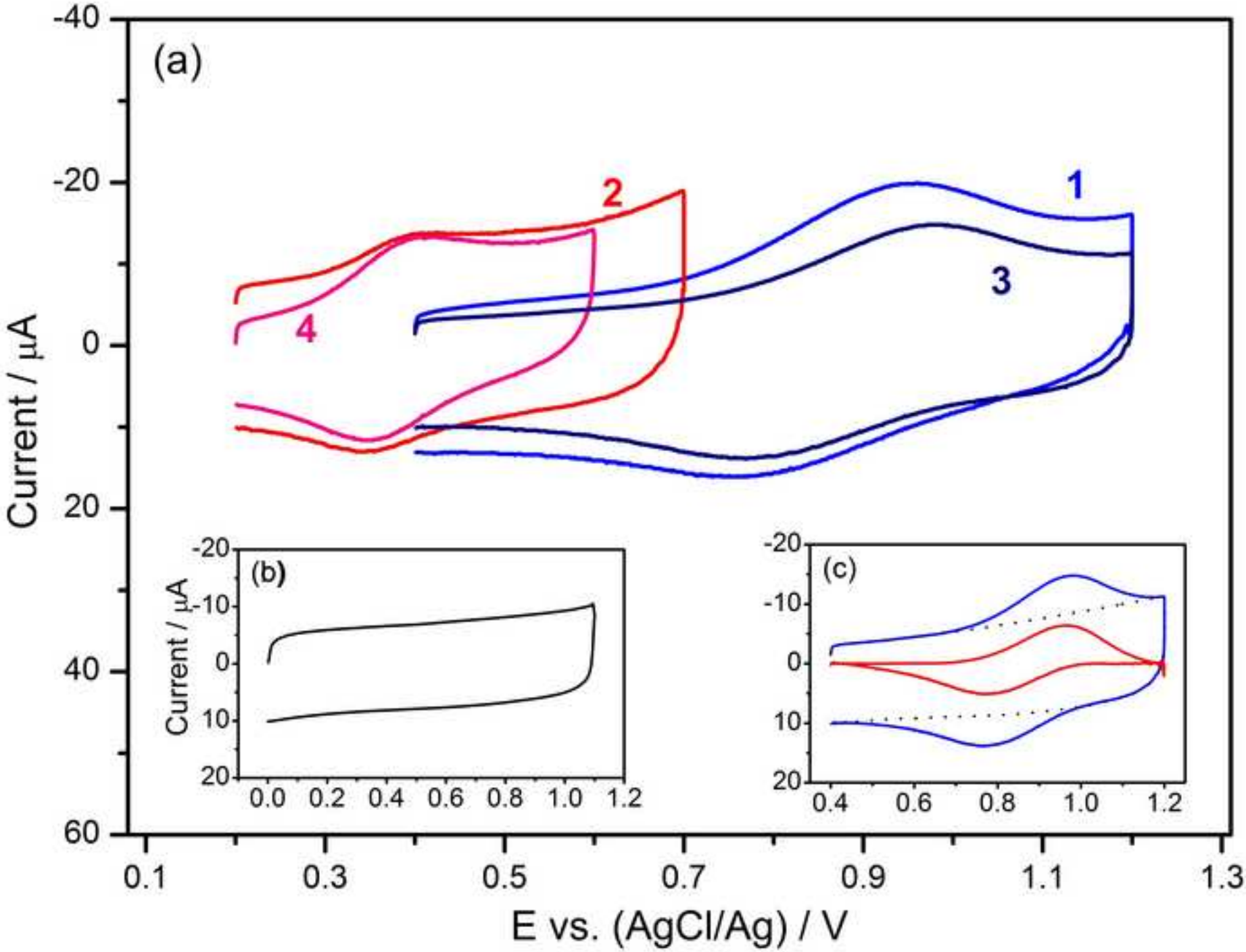

Figure 07(d)
Click here to download high resolution image

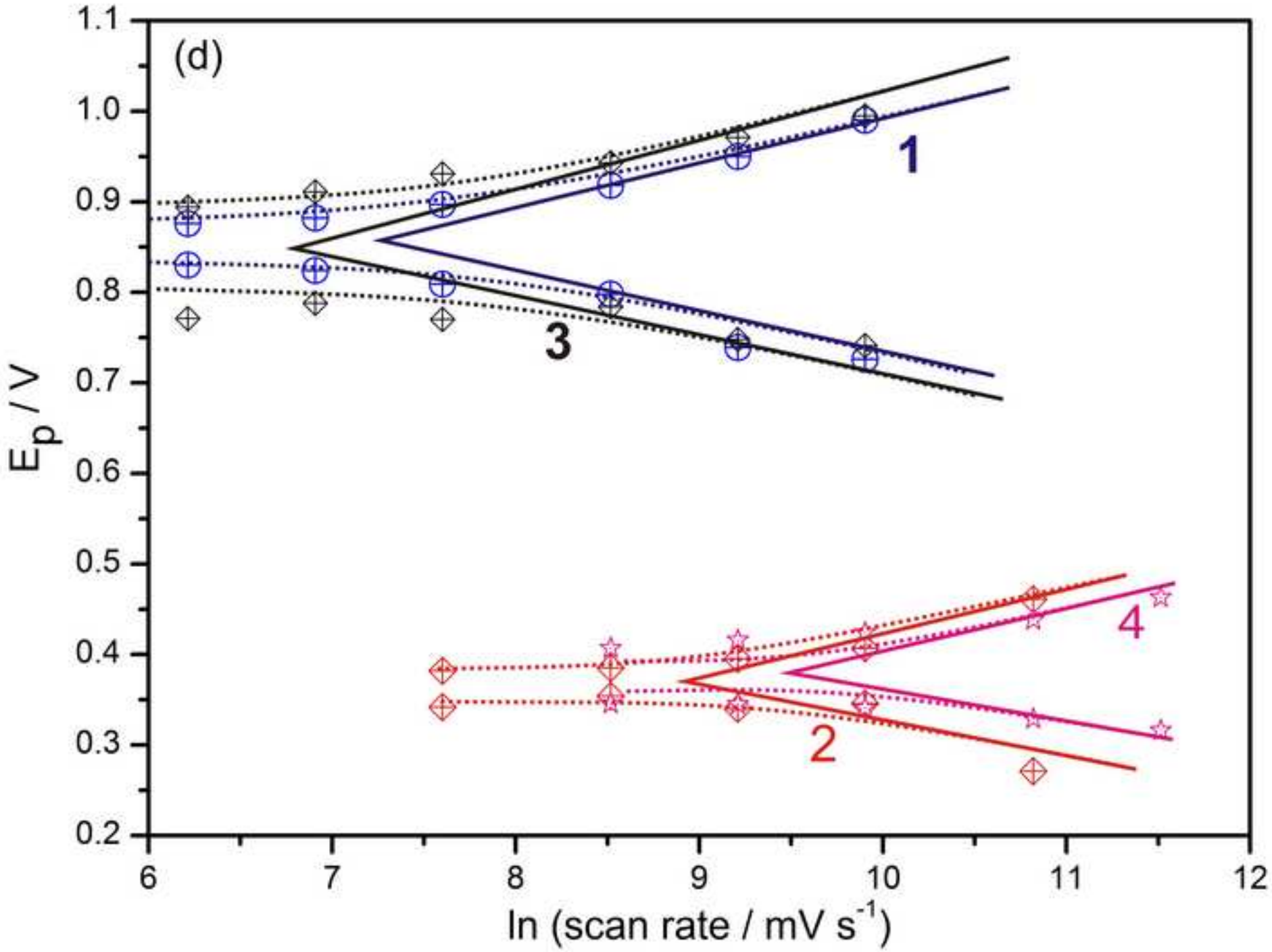

Figure 08(a)

Click here to download high resolution image

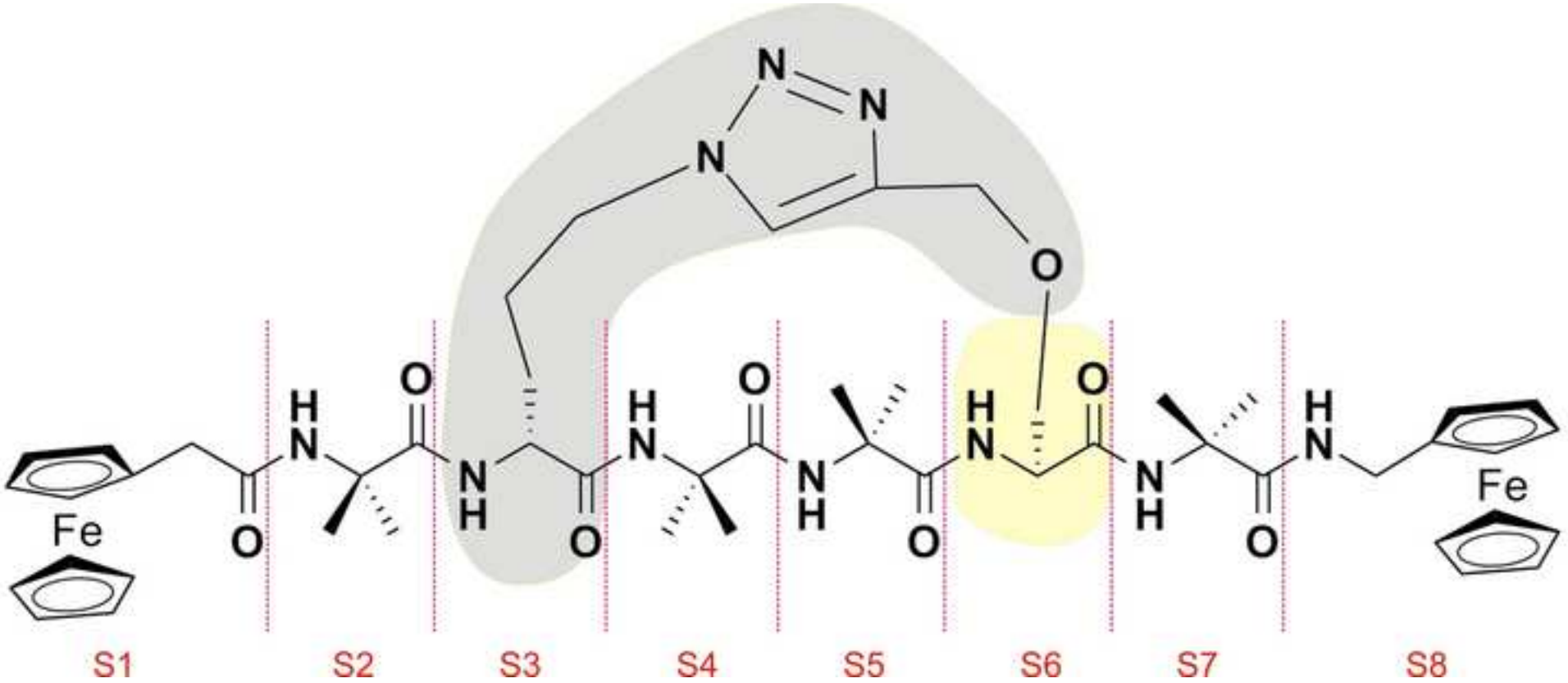

Figure 08(b)

Click here to download high resolution image

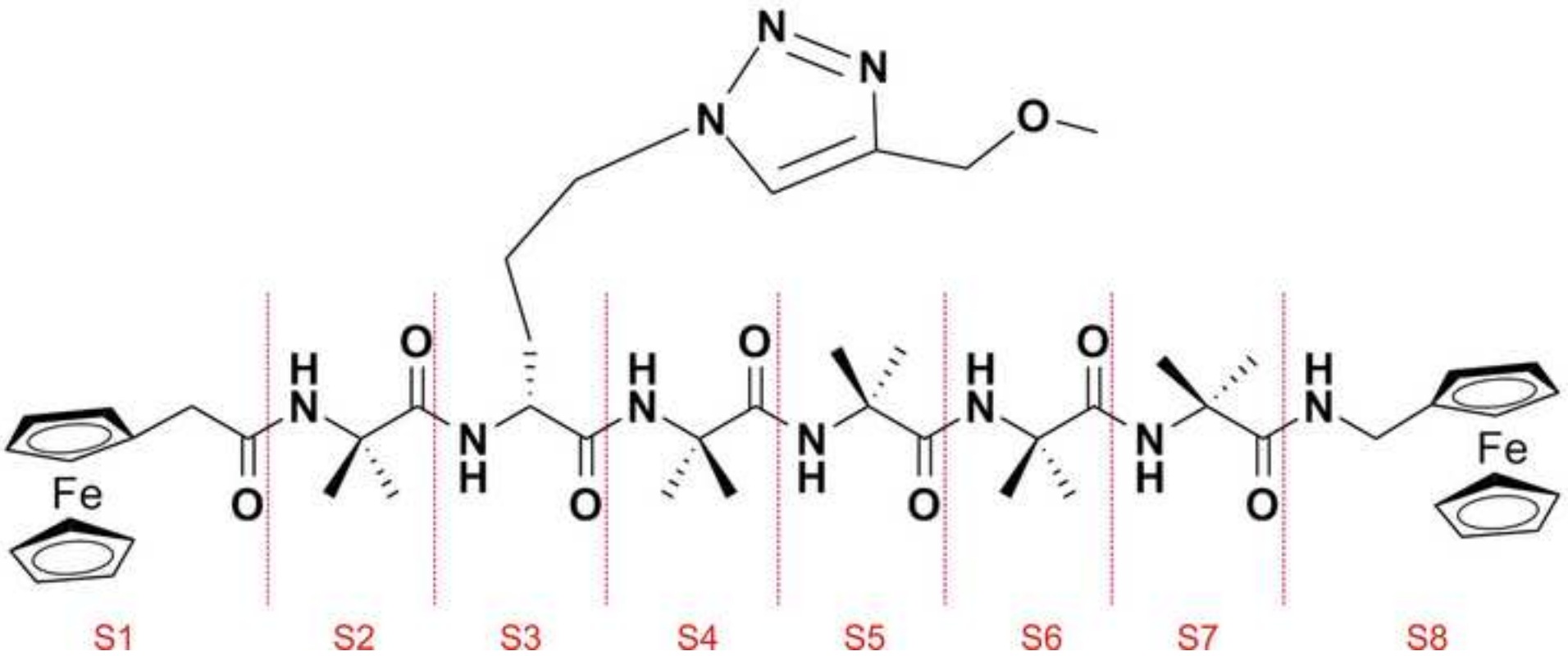

Figure 09(a)
Click here to download high resolution image

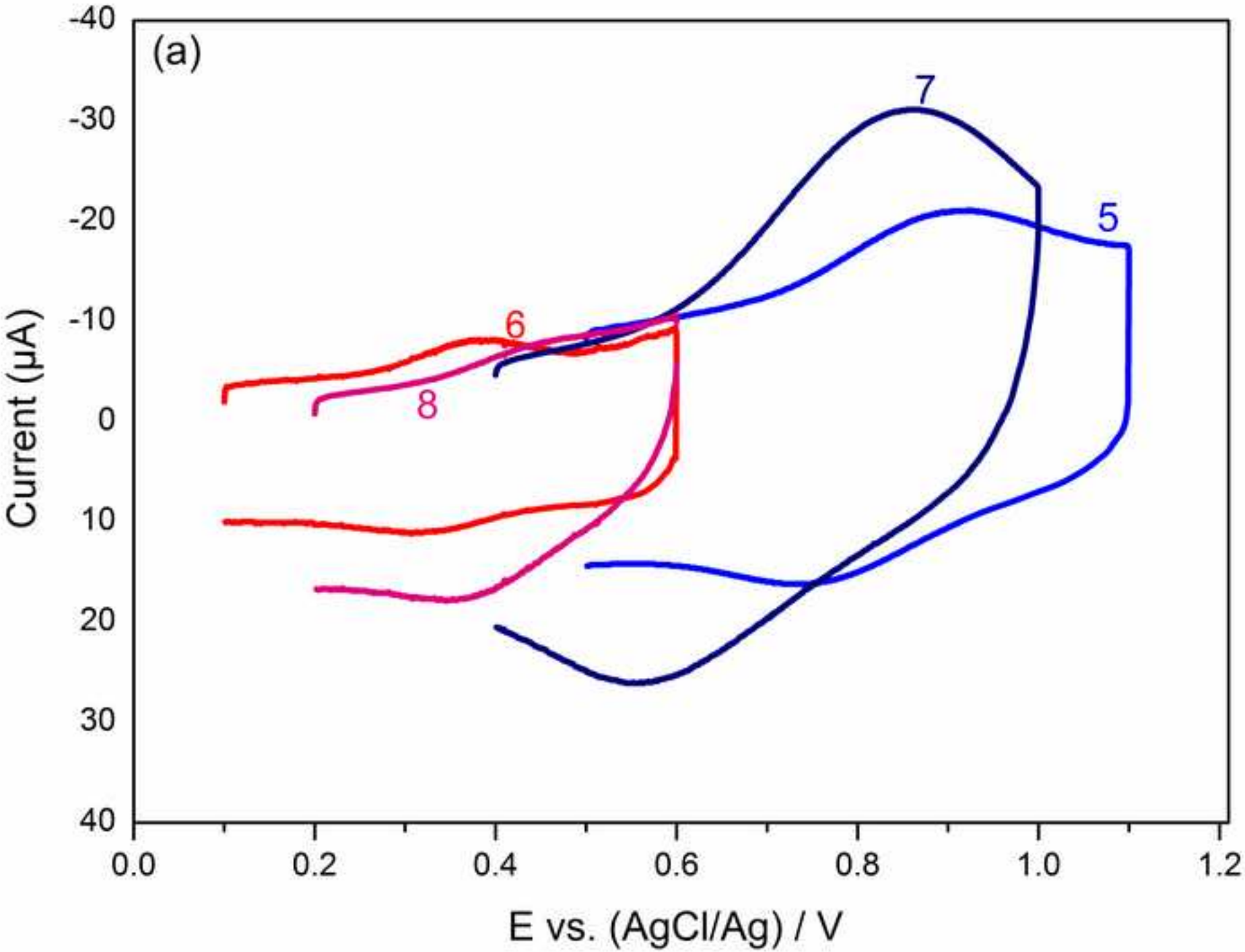

Figure 09(b)
Click here to download high resolution image

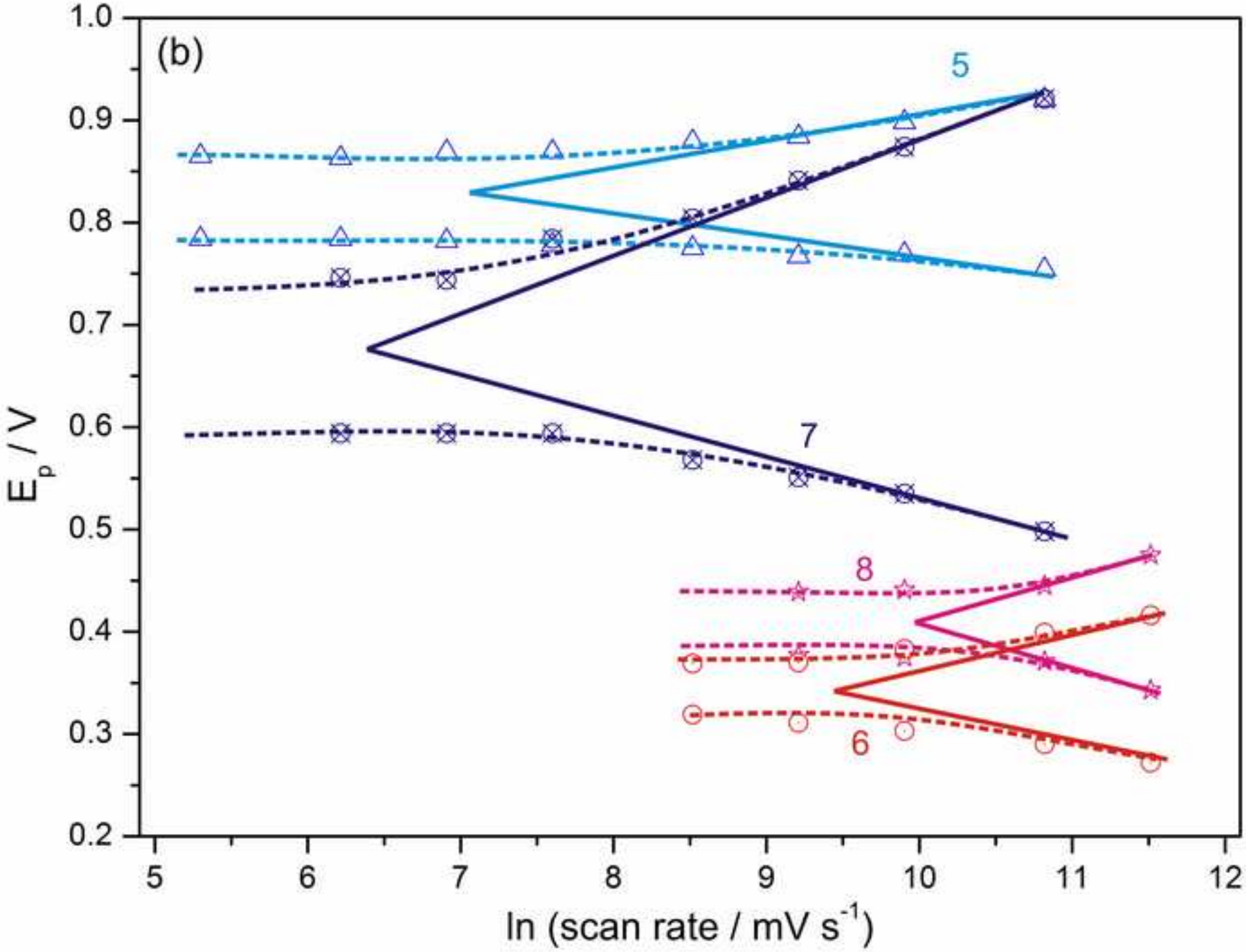

Graphical Abstract

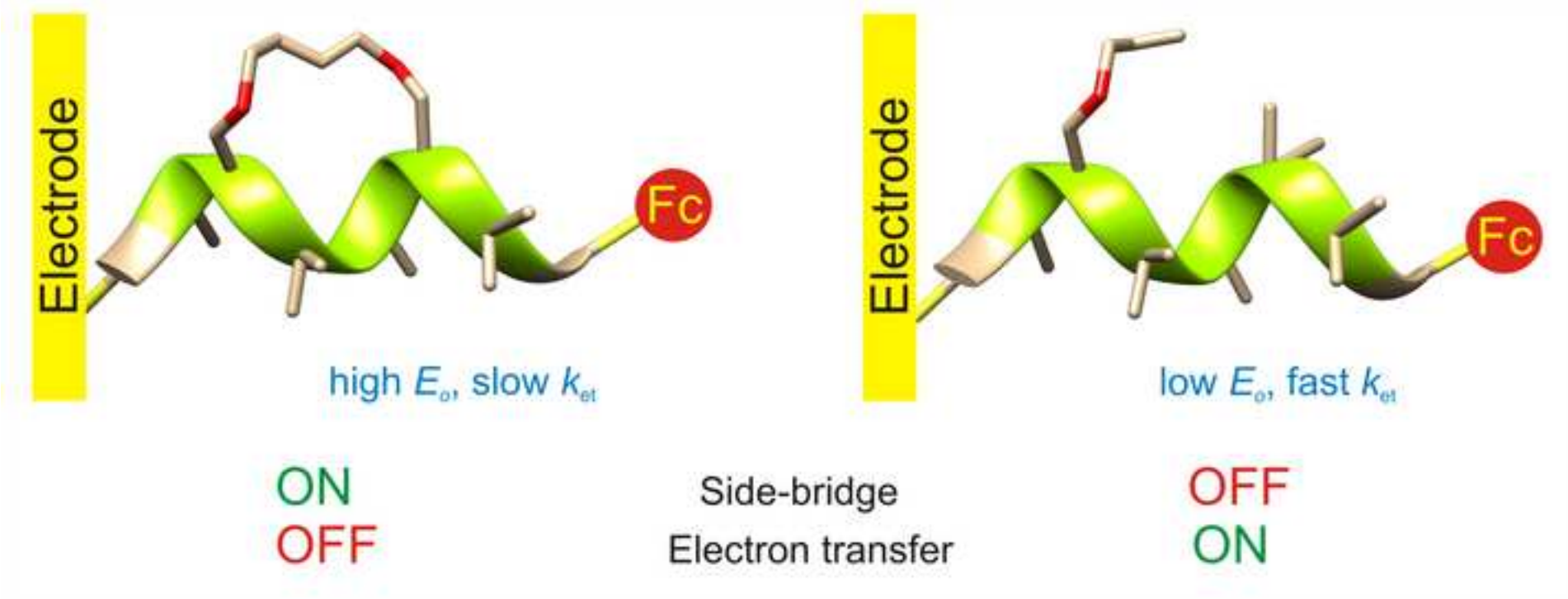

*Response to Reviewers

THE UNIVERSITY OF ADELAIDE AUSTRALIA

28/04/2016

Professor Sergio Trasatti

Department of Chemistry
University of Milan
20133, Milan
Italy

Dear Professor Trasatti,

Re: Manuscript ID: ISE15-11-06

Thank you for your communication of the 5th inst. We have acted on all the suggestions and comments raised by the reviewers to the best of our ability in the revised manuscript. Each point raised is specifically addressed below for clarity. All changes have been highlighted with a YELLOW background in the revised manuscript. Note that all references quoted in the letter have a consistent reference number cited in the revised introduction.

Reviewer #1:

(1) In the Introduction, the selection of references is definitely biased toward what the authors themselves did. For example, concerning the effect of peptide structure on electron tunneling no mention is made to the fundamental studies carried out by people such as Bilewicz, Sek, Kimura, Maran, Kraatz, Venanzi.

We have cited the following references contributed from Maran, Bilewicz, Sek, Kimura, Kraatz and Venanzi in the revised introduction, to appreciate their observations and insights on fundamental understanding of electron transfer in peptides. The references that already appeared in the first submission are marked with a symbol *.

[*9] A. Shah, B. Adhikari, S. Martic, A. Munir, S. Shahzad, K. Ahmad, H.-B. Kraatz, Electron transfer in peptides, Chemical Society Reviews, (2015) DOI: 10.1039/C1034CS00297K.
[10] F. Maran, C. Toniolo, Peptide and protein mediated electron and energy transfer, Biopolymers, 100 (2013) iii-iv.
[12] S. Sek, A. Sepiol, A. Tolak, A. Misicka, R. Bilewicz, Distance Dependence of the Electron Transfer Rate through Oligoglycine Spacers Introduced into Self-Assembled Monolayers, The Journal of Physical Chemistry B, 108 (2004) 8102-8105.
[13] Y. Arikuma, H. Nakayama, T. Morita, S. Kimura, Electron Hopping over 100 angstrom Along an alpha Helix, Angewandte Chemie-International Edition, 49 (2010) 1800.
[14] E. Gatto, M. Venanzi, Self-assembled monolayers formed by helical peptide building blocks: a new tool for bioinspired nanotechnology, Polymer Journal, 45 (2013) 468-480.
[16] J. Juhaniewicz, J. Pawlowski, S. Sek, Electron Transport Mediated by Peptides Immobilized on Surfaces, Israel Journal of Chemistry, 55 (2015) 645-660.
[*21] S. Yasutomi, T. Morita, Y. Imanishi, S. Kimura, A molecular photodiode system that can switch photocurrent direction, Science, 304 (2004) 1944-1947.

[28] S. Antonello, F. Formaggio, A. Moretto, C. Toniolo, F. Maran, Anomalous distance dependence of electron transfer across peptide bridges, Journal of the American Chemical Society, 125 (2003) 2874.
[29] F. Polo, S. Antonello, F. Formaggio, C. Toniolo, F. Maran, Evidence against the hopping mechanism as an important electron transfer pathway for conformationally constrained oligopeptides, Journal of the American Chemical Society, 127 (2005) 492.

(2) In other parts (p. 4), no references are provided to sustain sentences such as "... hydrogen bonding that are known to influence electron transfer." or ". in Fig. 1 contain Aib residues that are known to constrain the backbones into a well-defined 310-helix."

This part of the paragraph has been rewritten as below with newly added references and contents underlined.

> Here we present electrochemical studies on a series of synthetic peptides **1**-**8** to determine the influence of these effects on electron transfer, in isolation from other factors, such as chain length [27-29], dipole orientation [30,31] and the associated hydrogen bonding [32,33] that are known to influence electron transfer. Peptides **1**-**4**, as shown in Fig. 1 contain the geminally disubstituted residue, α-aminoisobutyric acids (Aib). They were used in the study since relatively short oligomers of Aib (3 or more units) are known to form predictable and particularly stable 3_{10}-helical structures.[28, 31, 34, 35] Thus, Aib-rich peptides made ideal model systems for investigating electrochemical mechanisms and kinetics in solution phase, demonstrated by previous pioneering work in this area.[28,29]

(3) Computational details are not provided.

Two new tables (i.e. Table 1 and 2) are included in the revised introduction to display detailed dihedral angles for all residues in the lowest energy conformers of helical peptides **1**-**4** (Table 1) and structural data for peptides **5**-**8** with comparison to optimal β-strand values(Table 2). Corresponding changes are also made in the revised text.

(4) The ohmic-drop correction is mentioned but not explained. In organic solvents this is a pretty complicated issue that is too often underestimated.

We had conversations on this technical issue with Professor David H Waldeck. It is worth mentioning that we are currently preparing a manuscript on “Cyclic voltammetric analysis of PNA and peptide monolayer electrode kinetics based on Marcus theory”. Relevant modifications are also made to reflect this new information in the revised text.

Prof Waldeck recommended his recently published review article “Fundamental studies of long- and short-range electron exchange mechanisms between electrodes and proteins in 'Applications of Electrochemistry and Nanotechnology in Biology and Medicine I', edited by N. Eliaz.” The following text in his article is helpful in addressing the referee’s comment. “When the conditions leading to large voltammogram distortions are unavoidable, the post measurement IRs drop corrections (where R_S is the solution resistance between the surface of the working electrode and the tip of the reference electrode) can be successfully applied through the electrochemical standard software programs to eliminate an error caused by the voltammograms distortion.” (Page 132 in his review) Also the peptides in the study are relatively small (3 or 6 residues), significantly smaller than cytochrome c. Thus we believe the ohmic-drop correction is not a big issue in the study.

(5) Calibration against ferrocene is mentioned but then all figures show the potentials against Ag/AgCl. Please show the CV curves versus ferrocene.

Ferrocene was used to calibrate the AgCl/Ag reference electrode after each experiment, but was not used as a reference electrode in the study. Indeed, the use of ferrocene as a reference electrode would badly interfere with the voltammetric measurements of ferrocene-derivatized peptides, and result in significant difficulty in electrochemical data analysis. To reflect the real condition in the study, we believe that it is more applicable to report potentials with respect to Ag/AgCl reference electrode.

(6) The conformation of peptides 1-4 was assessed by 1H NMR analysis. Further figures should be provided, at least as supporting information.

Since the journal Electrochimica Acta does publish online electronic supplementary information (https://www.elsevier.com/journals/electrochimica-acta/0013-4686/guide-for-authors, accessed on April 06, 2016), a typical CD spectrum for peptide 1 (as Fig.4a) and IR spectrum for peptide **8** (as Fig.4d) are included in the revised manuscript. Corresponding contents as the below are also added to the revised manuscript,

> A strong negative minimum near 202 nm, with a far weaker minimum at approximately 232 nm was observed in a representative CD spectrum of N-Boc protected peptide **1** (as shown in Fig.4a), which further supports a 3_{10}-helical conformation [36, 48].
>
> Amide I and II bands are used extensively in IR spectroscopy for peptide/protein structural determination. Typically for a β-strand conformation, a strong band (Amide I) is evident between 1612 and 1640 cm^{-1}, while another strong band (Amide II) is located between 1510 and 1530 cm^{-1}. Peptides **5**-**8** fall within this category, conforming their β-strand structure, with a representative spectrum (peptide **8**) shown in Fig. 4d. Amide A (N-H stretching) frequencies between 3277 and 3293 cm^{-1} were also observed in the IR spectra of peptides **5**-**8**, providing further evidence of structure [50].

(7) P. 8. The outcome is that no significant difference emerges. Is this 100% true? These calculations should play a key role in understanding what really makes the couple of corresponding peptides different.

Please refer to the two new tables (i.e. Table 1 and 2) for detailed geometric parameters of peptides **1**-**8.** Theoretical calculations were also included in the Results and Discussion section, in order to get insights into what makes electron transfer in constrained and linear peptides different.

(8) Section 3.2. How were the peptides "attached" to "vertically" (no image provided) aligned SWCNT array/gold? And how was the latter prepared?

The following text has been added to the Experimental section,

> *2.4. Preparation of ferrocene-derivatised peptide electrodes*
>
> P2-SWCNTs were functionalised using previously reported methods [41]. Shortened CNTs were then suspended in a solution of DMSO containing 0.2 mg mL^{-1} CNTs, 0.25 mg mL^{-1} DCC and 0.14 mg mL^{-1} DMAP. Polished flat gold disk electrodes were cleaned in 25 % v/v H_2O_2/ KOH (50 mM) for 20 min and then electrochemically cleaned by cycling between 0 and 1.5 V vs. Ag/AgCl in 50 mM KOH. This cleaning process yielded clean gold surfaces with peak separations of 59 mV in 1 mM $Ru(NH_3)_6^{+3/2}$ solution. The clean surfaces were then incubated in cysteamine for 24 h resulting in exposed amine groups. These substrates were then exposed to the functionalised

SWCNTs/DMSO suspensions for 24 h, after which they were rinsed with propan-2-ol and dried under nitrogen flow. The surfaces were then exposed to 0.01 M ferrocene-derivatised peptide in DMF solution containing 0.5 M HATU and 0.5 M DIPEA for 48 h before being further rinsed and dried. A typical AFM image of vertically aligned single-walled carbon nanotube array/gold (SWCNTs/Au) electrode (50×50 μm^2) is shown in Fig. 3. The average height of single-walled nanotubes is 206.9 nm. SWCNTs/Au electrodes were used in this study to provide a high surface concentration of redox probes, with an associated significant increase in sensitivity and reproducibility of the electrochemical measurement over bare Au electrodes [41-43].

(9) The title of section is inappropriate, unless the electrode is considered as part of the molecule. Please delete "Intramolecular".

The title of the section has been changed to “electron transfer in peptides”.

(10) For the density, one has to determine also the area of the electrode. How was it determined? How was background subtraction carried out? One should provide a figure showing both the background and the actual CV curves: very rarely the two traces overlap on the positive side. One cannot rely on an accurate determination (with far too many digits!) for peptide 8 or 7: in the first case, there is obviously another process occurring at 0.6 V, whereas for the latter I do not understand why the scan was reversed so early. The background should be the SWCNT array/gold system: how can that be so different for the various curves? This is obvious by inspection of the CVs in Figures 6a and 7a. The CVs, both background and in the presence of the peptide, should be provided at least up to 1.1 V.

Surface concentrations of attached peptides are determined based on the geometric area (0.33 cm^2) of flat gold disk electrodes.

Since single-walled carbon nanotube array/Au (SWCNTs/Au) electrodes were used in the cyclic voltammetric measurements, a large background (capacitive) current is always expected due to the rough surface of electrode. So it is quite often to see that two traces of cyclic voltammetric curve overlap on the positive side. A typical example is found in a highly cited article in this area, contributed by Gooding (J.J. Gooding, R. Wibowo, J.Q. Liu, W.R. Yang, D. Losic, S. Orbons, F.J. Mearns, J.G. Shapter, D.B. Hibbert, Protein electrochemistry using aligned carbon nanotube arrays, *Journal of the American Chemical Society*, 125 (2003) 9006-9007.). Due to its relatively large surface, this type of electrode can accommodate the binding of a large amount of peptides. This leads to improved reliability and reproducibility of the electrochemical response. Indeed, we used the same type of assembled carbon nanotube electrode in the study. These features can be further evidenced in two newly added insets in Fig 7, namely Fig 7b and c. Fig. 7b shows the cyclic voltammetric curve of SWCNTs/Au at 5 V s^{-1}. It is clear that a significant background current presents, with no redox peak observed in the potential range between 0 and 1.1 V. Fig. 7c demonstrates how background subtraction was carried out. After background subtraction, surface concentrations of the peptide can be determined by integrating faradaic current peak areas.

Electrochemical measurements of peptides **7** and **8** were conducted separately with a two-year time gap (2012 and 2014 respectively). We didn’t mean to set the same high potential sweep vertex when we carried out their cyclic voltammetric measurements. The cyclic voltammogram for peptide **8** presented in the first submission was wrong, which was recorded at a scan rate of 20 V s^{-1}. The right cyclic voltammogram for peptide 8 at a scan rate of 5 V s^{-1} is included in the revised manuscript.

(11) As for surface concentrations and formal potentials, the accuracy of the ET rate constants is far too large, particularly because of the lack of precise control of the ohmic-drop correction. Please also note that all these numbers are repeated so many times both in the text and the Tables.

Please refer to Point 4 above regarding the technical issue of ohmic-drop correction. Also, we deleted some repeated ET rate constants in the text.

(12) Why rate constants and formal potentials change? This is the main question.

The following text has been added to the Results and Discussion section, with newly added Figure 8 and Table 4.

> **T**heoretical calculations would provide further insight into the intramolecular electron transfer dynamics. Since single-step superexchange and multistep tunneling are widely accepted charge-transport mechanisms in peptides [11, 27, 56], we compared reorganisation energies for multiple sequential electron transfer steps along the helical peptide backbones. Peptides **9** and **10** were chosen for this study since they contain the same sequence as **1** and **2**, but with ferrocene units at both termini to act as both a donor and acceptor. Diabatic states were constructed by individually localizing an overall charge of 1 on each of the ferrocene units and amino acids, as shown in Fig. 8. The constrained peptide and its linear analogue show comparable reorganisation energies for all sequential tunnelling steps, except those providing a linking site for the side-bridge (i.e. S3). The reorganisation energies for the forward and backward electron steps from S3 in **9** are much higher than the corresponding steps in **10** (see Table 4). The introduction of the side-bridge gives rise to a significant increase in reorganisation energy, in the range of 3.14 – 6.97 kcal.mol^{-1}. The higher reorganisation energy barrier in peptide **9** is a direct result of the side-bridge constraint, thus further supporting our experimental results. Additionally, Maran [30] and Santi [31] showed that the direction of the associated dipole moment in a 3_{10}-helix could strongly influence the formal potentials. In particular, it is expected to stabilize the ferrocenyl group if the negative end of the dipole is adjacent to the ferrocene moiety. This would also push the oxidation of the ferrocene moiety toward more positive potentials.

Reviewer #2:

(1) In the experimental section the procedure adopted to realize the single-walled carbon nanotube array/gold electrodes and then to attach the peptides should be added; prior to the modification was the gold electrode subjected to any cleaning step?

A paragraph regarding "preparation of ferrocene-derivatised peptide electrodes" has been added as the Section 2.4 in the revised manuscript for detailed experimental information.

(2) In the paragraph 3.2, there is no mention of figure 6 (b) and figure 7 (b). A brief description of these figures is needed along with a comment on the high scan rate values employed.

The following sentences have been added to the text,

> This is clearly evidenced in the plot of peak potential versus ln(scan rate) as shown in Fig.7d, with a broad range of scan rate employed.
>
> The observed formal potentials (E_o) and apparent electron transfer rate constants (k_{et}) were estimated from the plot of peak potential versus ln(scan rate) as shown in Fig.9b and Table 5.

(3) In Figure 6(a) and 7(a), the pair of redox peaks have been attributed to the redox couple Fc+/Fc. Have the author verified the redox-inactive behavior of the peptide backbone?

No. A terminal ferrocenyl group is commonly used as a redox probe for electrochemical characterizations. In this study, only one pair of redox peaks were observed for all ferrocene-derivatised peptides. If any peptide backbone was electrochemically active, we would observe additional redox peaks.

(4) In Tables 1 and 2 how were the uncertainties associated to Surface concentration and ket derived? A note on the bottom of the tables should be appreciated.

A note as below is attached to Tables 3 and 4 (formerly Tables 1 and 2).

> Note: * Standard deviation with electrochemical measurements on three electrodes.

(5) The surface concentrations values reported in Table 2 are quite different. For example, passing from peptide 6 to peptide 7 the surface concentration goes from 2.73 to 9.21 (x10-10 mol.cm-2). How do the authors explain such differences?

This is attributed to two possible reasons. One is that these peptides have different molecular cross-sectional areas (perpendicular to the direction of peptide backbone); another could be due to the relatively more rough surface morphology of carbon nanotube array/Au electrode, in comparison to a flat electrode.

(6) For peptide 8 the electron transfer rate constant was 2-fold higher than that for peptide 6. For the authors this demonstrates the ability of the alkene groups to facilitate electron transfer through the peptide by acting as a "stepping stone". Could the phenol component contribute to facilitate electron transfer too?

The text has been amended to reflect this result.

(7) At page 14 line 36 "2-fold higher than that for 2" should be "2-fold higher than that for 6".

The text has been modified accordingly.

(8) In the text, references should precede punctuation marks.

The text has been modified accordingly.

Please don’t hesitate to contact me if you require any further clarification.

Yours sincerely,

JINGXIAN YU